# FTIR Spectrochemical Imaging Analysis of Lipid and Protein Content of Bottom-Ice Diatoms along a Tidal Strait within the Kitikmeot Sea, Canadian Arctic

by

Nicole M. Pogorzelec

A thesis submitted to the Faculty of Graduate Studies of

The University of Manitoba

In partial fulfilment of the requirements of the degree of

MASTER OF SCIENCE

Department of Environment and Geography

University of Manitoba

Winnipeg

# ABSTRACT

Within the ice bottom, ice algae begin their annual Arctic spring bloom in which they contribute up to half of the total annual primary production in the central Arctic Ocean. Essential fats (or lipids) are produced during the early portion of the ice algal bloom (e.g., polyunsaturated fatty acids (PUFAs) such as omega-3 fatty acids) and are of particular importance to the energy-rich Arctic marine ecosystem. Fourier Transform Infrared (FTIR) Spectrochemical imaging is an efficient and non-destructive analytical technique, which allows us to measure changes in ice algal biomolecular composition (i.e. saturated lipid, protein and biogenic silica). In this thesis, we examine diatom samples collected from first-year landfast sea ice across a tidal strait region located between the Finlayson Islands within Dease Strait of the Kitikmeot Sea, near Cambridge Bay, Nunavut, Canada. This research was conducted under the ICE-CAMPS (Ice Covered Ecosystem-Cambridge Bay Process Study) 2017 spring field campaign. It was determined, via two case studies:

i. the relative amount of biomolecular composition was a function of cell size and species.
ii. individual cell biomolecular composition trends were not depicted in bulk measurements (i.e. particulate organic carbon, chlorophyll *a*, etc.)
iii. Two expected nutrient gradients were observed within the tidal strait region, one spatially and one vertically
iv. lipid (protein) content increased (decreased) spatially in response to nutrient limitation, while lipid (protein) content increased (remained constant) vertically in the sea-ice

v. the creation of new FTIR imaging methods were successful in rapidly imaging the diatom community.

The findings presented here have reinforced the usefulness of the FTIR instrument to diatom autecological analysis. This sensitive, non-destructive and semi-quantitative analytical technique has allowed us to further our understanding not only of the ice algal community, but also the autecology of individual diatom taxa.

# ACKNOWLEDGMENTS

Thank you to my advisors, Dr. C.J. Mundy and Dr. Kathleen Gough for their continued support and guidance throughout my Master's Program and for the many exciting field-work opportunities I had the privilege to participate in. A special acknowledgment to my Advisory Committee members, Dr. Jason Morison and Wojciech Walkusz. This thesis successfully came together, due to their continued mentorship.

I'd like to extend a special thanks to everyone who participated in the ICE-CAMPS 2017 field season, especially Dr. Brent Else for his logistical support and Kwanwoo Kim and Sun-young Ha for their continued assistance in the field.

I would like to acknowledge and thank the Manitoba Government for awarding me the Manitoba Graduate Scholarship, the University of Manitoba Enhancement of the Tri-council (GETS), and the Northern Science Training Program (NSTP) for their financial support.

I'd also like to express my thanks and gratitude to my family and friends for their continued love and support throughout my Master's program. Thank you so much!

# TABLE OF CONTENTS

# LIST OF FIGURES

# LIST OF TABLES

# LIST OF SUPPLEMENTAL TABLES

# LIST OF COPYRIGHT MATERIAL

# CONTRIBUTION OF AUTHORS

The manuscript that comprises Chapter 3, titled "FTIR Autecological Analysis of Bottom-Ice Diatom Taxa across Nutrient Gradients in a Tidal Strait, Canadian Arctic", was a combined effort. As first author, I collected the samples in the field, analysed the samples using various analytical techniques and statistical approaches, constructed new and improved upon existing FTIR spectrochemical imaging techniques, compiled data into figures and tables, and prepared the draft manuscript. Dr. C.J. Mundy (last author) provided funding, field logistic and sampling support, constructive feedback, and guidance on the project. Dr. Kathleen Gough (second author) provided the FTIR instrument and provided constructive feedback and guidance on project and method development and on interpretation of FTIR data. Dr. Sun-Young Ha and Dr. Brent Else assisted with field logistics, sampling support and funding. Dr. Karley Campbell assisted with taxonomic analysis of lugol samples. All contributing authors reviewed and revised the manuscript before submitting it to the Journal of *Elementa: Science of the Anthropocene*.

# CHAPTER 1: INTRODUCTION

Attached to the bottom (skeletal) layer of sea ice, ice algae begin their bloom during the Arctic spring (Horner et al. 1992, Arrigo 2014, Leu et al. 2015). Ice algae can contribute up to half the total annual primary production in the central Arctic Ocean (Gosselin et al. 1997) and their average contribution in the surrounding shelf seas is estimated at 3-25% (e.g., Legendre et al. 1992, Michel et al. 2006, Leu et al. 2015). Their ecological role as the primary source of photosynthetic production during the early spring best encapsulates their importance to the ecosystem. Energy-rich lipids are produced during the early portion of the ice algal bloom (e.g., long chain omega-3 fatty acids or polyunsaturated fatty acids (PUFAs); Mock & Thomas 2005, Leu et al. 2010, Søreide et al. 2010), and are of particular importance to the energy demanding Arctic marine ecosystem (Michel et al. 2006, Søreide et al. 2010, Arrigo 2014).

Increasing Arctic temperatures, declining sea ice extent and thickness, later freeze-up and an earlier, but longer ice melting seasons (Comiso et al. 2008, Markus et al. 2009, Stroeve et al. 2012, NSIDC 2016) are rapidly changing the ice algal environment. Later winter sea ice formation has also been observed to influence the accumulation of ice algal assemblages. This delay reduces the ice algal seeding potential, by an overall reduction in suspended ice algal standing stock during late winter (Niemi et al. 2011). During spring, the potential for increased UV-radiation exposure (Bernhard et al. 2013) as well as increase in the overall light intensity to the bottom ice algal community will occur with changes to snow and sea ice thickness, due to an earlier melting season. This increase in radiation and light exposure affects ice algal growth (Leu et al. 2007), as well as their nutritional PUFA content (Leu et al. 2010). Model predictions have also indicated that primary production increases in the water column with early melt, versus that

of sea ice (Arrigo et al. 2008, Kahru et al. 2011, Tedesco et al. 2019). The lipid-rich ice algal bloom is also an important food source for marine-based grazers. Based on an assumed bottom-up driven food-web, it has been hypothesized that early bloom termination can negatively impact the overall Arctic marine food-web because of a mis-matched trophic cascade (Søreide et al. 2010).

During the initial part of a high Arctic spring bloom (late March – early April; Cota et al. 1991; Leu et al. 2015), ice algae are light-limited (Gosselin et al. 1990). This light limitation is a combination of a low seasonal solar angle and the strong light attenuation properties of snow and sea ice (Perovich et al. 1998). Algal photosynthetic processes can be greatly limited at this time with a reduction in cellular inorganic carbon assimilation (i.e. conversion of inorganic carbon to organic carbon), leading to a reduction in cellular lipid production, cell growth, and overall cell biomass accumulation (Mock & Gradinger 2000, Mock & Kroon 2002a, b). Because of this seasonal limitation, the bottom ice algal community photo-acclimates. This is achieved by either increasing their total content of cellular photosynthetic pigments under low light to increase production or decreasing their chloroplast volume under high light to prevent light stress (Gosselin et al. 1990, Kirst & Wiencke, 1995). Near the end of the ice algal bloom (late May-early June; Cota et al. 1987, Leu et al. 2015), insolation increases, while snow albedo decreases. The increase in light availability and/ or photosynthetically active radiation (PAR; 400-700 nm waveband) to the bottom ice algal community (Mundy et al. 2005, Leu et al. 2015) increases cellular photosynthetic lipid production.

Light availability is not the sole limiting factor for ice algal growth. Lack of essential under ice nutrients, such as dissolved inorganic nitrogen, phosphorous and silica, can limit ice algal growth and potentially terminate the spring bloom (Gosselin et al. 1990, Smith et al. 1997, Leu et

al. 2015). Generally, dissolved nitrogen (e.g., nitrate, nitrite, and ammonium) is the first nutrient to become limiting during the transition to the end of the bloom (Gosselin et al. 1990, Smith et al. 1997, Leu et al. 2015). Nitrogen plays a significant role in both cellular protein and lipid production. When nitrogen is available to the bottom ice algal community, nitrogen will be allocated into cellular protein production. However, when nitrogen becomes limiting, protein production is reduced and a greater allocation of carbon to lipid production occurs (Smith et al. 1997, Mock & Kroon 2002a, Pogorzelec et al. 2017).

There are several ways in which nutrients are transported to the ice algal community, such as regeneration of inorganic nutrients from recycled bio-organic material (i.e. algae, bacteria, other organism detritus), sea water exchange during desalination of sea ice (Reeburgh 1984) and water column mixing, via eddy diffusion across the ocean-ice boundary layer (Meguro et al. 1967, Cota et al. 1987). Recently, a constricted tidal strait (i.e., shallow and narrow waterways that confines the regular flow of water) has been observed to exhibit strong surface currents that appear to increase the accumulation of ice algal biomass further up into the sea ice compared to landfast ice away from the strait (Dalman et al. 2019). In the latter work, it was hypothesized that turbulence in tidal straits increased nutrient exchange within the bottom ice environment, such that the nutrients augmented algal growth higher up into the ice cover. These recent observations are currently under investigation in order to improve our understanding of ocean-ice nutrient fluxes with regards to tidal strait surface currents, ocean-ice turbulent exchange, and impacts on algal growth and accumulation. However, more information is required on vertical resolution of algae within the bottom ice sections and their nutritional status.

Fourier Transform Infrared (FTIR) spectrochemical imaging is a non-destructive analytical technique that has been previously demonstrated to be effective and efficient for the detection of

algal biomass composition (Heraud et al. 2007, Sackett et al. 2014, 2016, Pogorzelec et al. 2017). Lipid production is greatly affected by the amount of light available under the sea ice (Gosselin et al. 1990, Mock & Gradinger 2000, Mock & Kroon 2002a, b), whereas protein content is generally affected by the amount of available nutrients to the ice algal community (Gosselin et al. 1990, Mock & Kroon 2000a). Therefore, lipid ($CH_2$+$CH_3$ spectral bands) and protein (Amide I spectral band) content have been theorized to act as both light and nutrient availability biomarkers, respectively, and can be monitored over time for individual diatom taxa throughout their bloom period.

## 1.1 STATEMENT OF PURPOSE

Ice algae are a critical component of the Arctic marine ecosystem, yet we lack a full understanding of algal autecology, which impedes our ability to predict the ecosystem's response to ongoing climate change. The purpose of this study is to determine the influence of nutrient fluxes on biomass composition of individual Arctic diatom cells in comparison to the bulk biomass and species composition of their natural community, during the spring ice algal bloom.

## 1.2 OBJECTIVES

This study was performed on diatom samples collected from first-year landfast sea ice across the Finlayson Island's tidal strait within Dease Strait of the Kitikmeot Sea, near Cambridge Bay, Nunavut, Canada, under the ICE-CAMPS (Ice Covered Ecosystem-Cambridge Bay Process Study) field campaign during the spring of 2017. My objectives, including linked testable hypotheses, are to:

(i) examine the contribution of single cell relative biomolecular composition (lipids and proteins) from different diatom taxa (i.e. *Nitzschia frigida* and *Attheya* spp.), using FTIR microscopy

*H.1 Algal community FTIR-derived biomolecular composition will be a function of cell size*

(ii) examine the relationship between FTIR-derived biomolecular composition of diatoms (objective 1) to that of the ice algal community, via bulk filter-based measurements (e.g. pigments, particulate organic carbon, taxonomic composition, etc.) and

*H.2 FTIR-derived biomass composition will be directly related to bulk filter-based measurements and taxonomic composition*

(iii) relate these changes in biomolecular composition to variation in light intensity and nutrient flux across a vertical gradient within the ice-bottom habitat and spatial gradient within a tidal strait.

*H.3 Lipid content will increase in response to increased light availability and decreased nutrient supply*

*H.4 Protein content will increase in response to decreased light availability, but will decrease when nutrients become limiting*

*H.5 A gradient of increasing light availability and decreasing nutrient supply from the ocean-ice interface and up into the ice bottom will drive changes in biomass composition according to H.3 and H.4*

*H.6 A greater nutrient flux that occurs towards the centre of a tidal strait where under-ice currents increase will drive changes in biomass composition according to H.3 and H.4.*

Furthermore, recognizing the useful and rapid measurement capacity of an FTIR instrument, the final objective is to:

(iv) design a methodology for rapid spectrochemical imagining acquisition of the biomolecular composition of the diatom bulk community, as opposed to individual cell analysis in objective 1.

## 1.3 THESIS LAYOUT

This thesis is formatted in the style of a sandwich thesis and is comprised of 5 chapters. This introductory chapter includes a short synopsis on the importance of the research, a list of objectives and corresponding hypotheses, and the thesis layout. Chapter 2 provides the background information essential to understanding the methodology of Chapters 3 and 4, through a literature review of ice algae, light and nutrient availability and the fundamentals of FTIR spectrochemical imaging. In Chapter 3 is an integration of thesis objectives 1, 2, and 3 and the underlying hypotheses. I examine the influence of under-ice currents within a tidal strait region on individual diatom taxa biomolecular composition, filter-based ice algal community measurements and taxonomic composition, light and nutrient availability, and cell location within the strait and sea ice. This chapter is presented as a peer-reviewed manuscript and has been submitted to *Elementa: Science of the Anthropocene*:

Pogorzelec, N.M., Gough, K.M., Ha, S.Y., Campbell, K., Kim, K., Else, B., and Mundy, C.J., (2019) FTIR autecological analysis of bottom-ice diatom taxa across nutrient gradients in a tidal strait, Canadian Arctic. *Elementa: Science of the Anthropocene* (in review).

Objective 4 is accomplished in Chapter 4 by constructing and expanding upon various FTIR imaging methods, with the goal of developing a rapid method for analysis of changes in biomolecular composition in the diatom community. In Chapter 5, I conclude the thesis by summarizing key conclusions and providing future recommendations for the application of FTIR spectroscopy in support of ice algae, and more generally, diatom autecological research.

# 1.4 REFERENCES


Arrigo, K.R., (2014) Sea ice ecosystems. Annu. Rev. Mar. Sci., 6:439-67. doi: 10.1146/annurev-marine-010213-135103

Arrigo, K.R., van Dijken, G., and Pabi, S., (2008) Impact of a shrinking Arctic ice cover on marine primary production. Geophysical Research Letters, 35: L19603. doi: 10.1029/2008GL035028

Bernhard, G., Dahlback, A., Fioletov, V., Heikkilä, A., Johnsen, B., Koskela, T., Lakkala, K., and Svendby, T., (2013) High levels of ultraviolet radiation observed by ground-based instruments below 2011 Arctic ozone hole. Atmos. Chem. Phys. 1:10573-10590

Comiso, J.C., Parkinson, C.L., Gersten, R. and Stock, L., (2008) Accelerated decline in the Arctic sea ice cover. Geophys. Res. Lett., 35: L01703. doi: 10.1029/2007GL031972

Cota, G.F., Prinsenberg, S.J., Bennett, E.B., Loder, J.W., Lewis, M.R., Anning, J.L., Watson, N.H.F. and Harris, L.R., (1987) Nutrient fluxes during extended blooms of Arctic ice algae. Journal of Geophysical Research, 92: 1951-1962

Cox, G.F.N. and Weeks, W.F., (1988) Numerical simulations of the profile properties of undeformed first-year sea ice during the growth season. Geophysical Research, 93: 12,449-12,460

Dalman, L.A., Else, B.E., Barber, D., Carmack, E., Williams, W.J., Campbell, K.,
Duke, P.J., Mundy, C.J. (2019) Enhanced ice algal biomass along tidal strait in the lower NW Passage. Elementa: Science of the Anthropocene.

Gosselin, M., Legendre, L., Therriault, J.C. and Demers, S., (1990) Light and nutrient limitation of sea-ice microalgae (Hundson Bay, Canadian Arctic). J. PhycoL, 26:220-232

Gosselin, M., Legendre, L., Therriault, J.C. and Demers, S., (1997) New measurements of phytoplankton and ice alga production in the Arctic Ocean. Deep-Sea Research Ii, 44(8):1623-1644

Heraud, P., Wood, B.R., Beardall, J. and McNaughton, D., (2007) Probing the Influence of the Environment on Microalgae Using Infrared and Raman Spectroscopy. New Approaches in Biomedical Spectroscopy. American Chemical Society, Washington, DC, 85-106

Horner, R., Ackley, S.F., Dieckmann, G.S., Gulliksen, B., Hoshiai, T., Legendre, L., Melnikov, I.A., Reeburgh, W.S., Spindler, M. and Sullivan, C.W., (1992) Ecology of sea ice biota: 1. Habitat, terminology, and methodology. Polar Biol, 12:417-427

Kahru, M., Brotas, V., Manzano-Sarabia, M., and Mitchell, B.G. (2011) Are phytoplankton blooms occurring earlier in the Arctic? Global Change Biology, 17:173-1739

Kirst, G.O. and Wiencke, C., (1995) Ecophysiology of Polar Algae. J Phycol 51(2):181-199

Legendre, L., Ackley, S.F., Dieckmann, G.S., Gulliksen, B., Horner, R., Hoshiai, T., Melnikov, I.A., Reeburgh, W.S., Spindler, M. and Sullivan, C.W., (1992). Ecology of sea ice biota: 2. Global significance. Polar Biology, 12(3-4):429-444.

Leu, E., Wängberg, S.Å., Wulff, A., Falk-Petersen, S., Ørbæk, J.B. and Hessen, D.O., (2007) Effects of changes in ambient PAR and UV radiation on the nutritional quality of an Arctic diatom (Thalassiosira Antarctica var. borealis). Journal of Experimental Marine Biology And Ecology, 337:65-81

Leu, E., Wiktor, J., Søreide, J.E., Berge, J. and Falk-Petersen, S., (2010) Increased irradiance reduces food quality of sea ice algae. MEPS, 411:49-60

Leu, E., Mundy, C.J., Assmy, P., Campbell, K., Gabrielsen, T.M., Gosselin, M., Juul-Pedersen, T. and Gradinger, R., (2015) Arctic spring awakening-steering principles behind the phenology of vernal ice algae blooms. Progress in Oceanography, 139:151-170

Markus, T., Strieve, J.C., and Miller, J., (2009) Recent changes in Arctic sea ice melt onset, freezeup, and melt season length. Journal of Geophysical research, 114:C12024

Meguro, H., Ito, K. and Fukushima, H., (1967) Ice flora (bottom type): a mechanism of primary production in polar seas and the growth of diatoms in sea ice. Arctic, 114-133.

Michel, C., Ingram, R.G., Harris, L.R. (2006) Variability in oceanographic and ecologicl processes in the Canadian Arctic Archipelago. Progress in Oceanography, 71:379-401

Mock, T., and Kroon B., (2002a) Photosynthetic energy conversion under extreme conditions-I: important role of lipids as structural modulators and energy sink under N-limited growth in Antarctic sea ice diatoms. Phytochemistry, 61:41-51

Mock, T., and Kroon, B., (2002b) Photosynthetic energy conversion under extreme conditions-II: the significant of lipids under light limited growth in Antarctic sea ice diatoms. Phytochemistry, 61:53-60

Mock, T., Thomas, D.N., (2005) Recent advances in sea-ice microbiology. Environmental Microbiology, 7(5):605-619

Niemi, A., Michel, C., Hille, K. and Poulin, M., (2011) Protist assemblages in winter sea ice: setting the stage for the spring ice algal bloom. Polar Biology 34:1803-1817

NSIDC (2016) Daily image update. Accessed on June 13 2016. Nsidc.org/arcticsciencenews/

Perovich, D.K., Roesler, C.S. and Pegau, W.S., (1998) Variability in Arctic sea ice optical properties. Journal of Geophysical Research 103:1193-1208

Pogorzelec, N.M., Mundy, C.J., Findlay, C.R., Campbell, K., Diaz, A., Ehn, J.K., Rysgaard, S. and Gough, K.M., (2017) FTIR imaging analysis of cell content in sea-ice diatom taxa during a spring bloom in the lower Northwest Passage of the Canadian Arctic**.** MEPS, 69:77-88

Reeburgh, W.S., (1984) Fluxes associated with brine motion in growing sea ice. Polar Biology, 3(1):29-33

Sackett, O., Petrou, K., Reedy, B., De Grazia, A., Hill, R., Doblin, M., Beardall, J., Ralph, P. and Heraud, P., (2014) Taxon-specific responses of Southern Ocean diatoms to Fe enrichment reveale by synchrotron radiation FTIR microscopy. Biogeoscience, 11:5795-5808.

Sackett, O., Petrou, K., Reedy, B., Hill, R., Doblin, M., Beardall, J., Ralph, P. and Heraud, P., (2016) Snapshot prediction of carbon productivity, carbon and protein content in Southern Ocean diatom using FTIR spectroscopy. The ISME Journal 10:416-426

Smith, R.E.H., Gosselin, M. and Taguchi, S., (1997) The influence of major inorganic nutrients on the growth and physiology of high arctic ice algae. Journal of Marine Systems 11:63-70

Søreide, J.E., Leu, E.V.A., BERGE, J., Graeve, M. and FALK-PETERSEN, S.T.I.G., (2010) Timing of blooms, algal food quality and Calanus glacialis reproduction and growth in a changing Arctic. Global Change Biology 16:3154-3163

Stroeve, J.C., Serreze, M.C., Holland, M.M., Kay, J.E., Malanik, J., and Barrett, A.P., (2012) The Arctic's rapidly shrinking sea ice cover: a research synthesis. Climate Change 110:1005-1027, doi 10.1007/s10584-011-0101-1

Tedesco, L., Vichi, M., Scoccimarro, E., (2019) Sea-ice algal phenology in warmer Arctic. Science Advances. 5(5): EAAV4830. DOI: 10.1126/sciadv.aav4830

# CHAPTER 2: LITERATURE REVIEW

## 2.1 DIATOM HABITAT & CHARACTERISTICS

### *2.1.1 Habitat and Colonization*

Ice algae can be found in both the Arctic and Antarctic, growing at the edges of available algal habitats on Earth. Ice algae's vertical distribution within sea ice varies and depends on the seeding mechanism. The detailed review by Horner et al. (1992) describes the vertical distribution of ice algae (Fig. 2.1). Briefly, in the Antarctic, ice algae have been observed to occupy the surface (infiltration, deformation, and melt pond communities), interior (freeboard and channel communities), and the bottom (interstitial and platelet communities) of sea ice. However, in the Arctic, infiltration, freeboard and platelet communities are either rare (McMinn & Hegseth 2004; Fernandez-Mendez et al., 2018) or not found within the sea ice (Syvertsen 1991, Horner et al. 1992, Ackley et al. 1994).

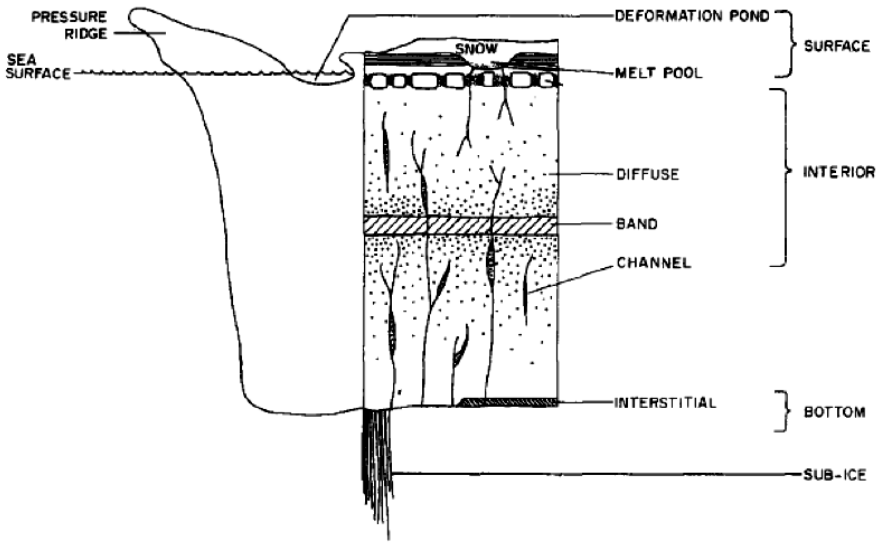


**Figure 2. 1:** Vertical distribution of ice algae. Modified Horner et al. (1992). Copyright © Springer Nature (1992).

Garrison et al. (1983) proposed that during the initial formation of sea ice, especially in turbulent waters, frazil ice forms and traps particles within the water column, incorporating these particles within the sea ice's crystalline substructure. They suggested that this was the likely mechanism by which surface ice algae are incorporated into sea ice (Garrison et al. 1983, Spindler 1994, Gradinger & Ikävalko 1998). This was later confirmed by Garrison et al. (1989) as a possible process through laboratory experiments. Niemi et al. (2011) found ice algae colonization to be a function of the freeze-up date, with more abundant and diverse communities found in ice formed during fall instead of late winter when fewer cells are found in the upper water column. Syvertsen (1991) proposed an alternative mechanism by which ice algae can be enriched into the sea ice by a process of under-ice wave action or increased current, for which the process was examined in detail by Weissenberger & Grossmann (1998). They noted that during laboratory experiments, where a current was generated under newly forming sea ice, the concentration of algal biomass within the sea ice significantly increased (Ackley et al. 1987, Spindler 1994, Gradinger & Ikävalko 1998, Weissenberger & Grossmann 1998). In the Antarctic, Dayton et al. (1969) observed another mechanism in which the upwelling-transport of benthic organisms to the platelet ice layer occurred. Anchor ice, which forms at the ocean floor, can detach from the bottom and ascend to the surface, resulting in the transportation and incorporation of benthic organisms into the sub-platelet ice layer. More recently, Olsen et al. (2017) suggested a role of ice algae release from old ice acting to seed younger adjacent sea ice floes. Environmental factors also influence the distributions of ice algae within the sea ice, such as nutrients, light availability (Smith et al. 1990), temperature and brine salinity (Arrigo & Sullivan 1992).

### *2.1.2 Diatoms: Characteristics of the dominant ice algal taxa*

Bacillariophyceae (common name: diatom) are the dominant taxa of ice algae, making up more than half of the ice algal community (Poulin et al. 2011), and contributing more than 70% of the total algal carbon within sea ice (Gosselin et al. 1997, Gradinger 1999). These specific algal taxa also serve as the main pulse of photosynthetic production, providing nourishment to an energy-rich lipid driven marine food web (Leu et al. 2015). Diatoms are unique unicellular photosynthetic microorganisms that can range from 2 μm to > 1 mm in size. They are encased in an opal shell (silicon dioxide) called a frustule. The frustule consists of two overlapping valve pieces, where one valve is larger (epitheca) than the other (hypotheca). The epitheca and hypotheca valves act as a "lid and box", respectively (Crawford 1981, Kröger 2007). Diatom identification is mainly based on their frustule morphology, rather than on DNA or chemical analysis. Morphological identifiers include frustule decoration, patterns, and symmetry, with pennate (bilateral frustule symmetry) diatoms being the dominant taxa in Arctic ice algal communities (Round et al. 1990, Różańska et al. 2009, Poulin et al. 2011). However, sometimes centric (radial frustule symmetry) diatoms can become more prevalent and even dominant in nutrient-depleted or higher-light conditions (Różańska et al. 2009, Campbell et al. 2016).

## 2.2 SOLAR IRRADIANCE AND NUTRIENT FLUXES

### *2.2.1 Solar Irradiance*

High Arctic ecosystems are controlled by the amount of incoming solar radiation or light availability. This is especially important during the winter-spring seasonal transition, specifically Phases I (pre-bloom) and II (bloom period) of the ice algal bloom cycle (Figure 2.2; Leu et al. 2015). Phase I or the pre-bloom phase occurs during the winter months, where light availability

is either extremely limited or non-existent, and ice algae remain in a net heterotrophic state. Phase II occurs once a critical light threshold is passed and is sufficient enough for under-ice algal production (0.36 – 9 μmol photon m-2 s-1; Horner & Schrader 1982, Mock & Gradinger 1999). This in turn signifies the end of the winter season and the start of the spring ice algal bloom, when ice algae transition towards a net autotrophic state (Leu et al. 2015). Subsequently, Phase II ends (bloom termination) when the water column nutrients become exhausted and warming temperatures result in brine channel drainage, expelling the sympagic community (Leu et al. 2015).

During the initial part of Phase II, sea ice, trapped in-ice sediments, and overlying snow cover can influence light availability and impede the ice algae's overall growth, production and taxonomic composition (Mundy et al. 2005, Różańska et al. 2009, Juhl & Krembs 2010, Alou-Font et al. 2013). For example, Mundy et al. (2005) examined three snow cover depths (thin (<6 cm), medium (6 to 20 cm) and thick (>20 cm)), which could be easily identified based on the variation in Chl *a* concentration (greater biomass under thin snow cover vs. thick snow cover). However, this variation in Chl *a* concentration under varying snow depths could only be observed in the earlier parts of the bloom. This is in part due to the high albedo and attenuative properties of snow and sea ice, with snow cover being the strongest attenuator of light transmitted to the underlying ice algal community (Perovich et al. 1998, Mundy et al. 2005). Snow has a high albedo (0.8 to 0.9) and an attenuation coefficient that can be more than an order of magnitude greater than that of sea ice (Perovich et al. 1998). This was observed by Cota (1985), who noted a significant reduction in light transmission under thick snow (20 cm) cover versus that of thin snow cover (3 cm) and bare ice (0 cm; also noted by Mundy et al. 2005, Różańska et al. 2009). Furthermore, snow grain size increases, as the solar angle increases

towards the summer solstice and the attenuation coefficient of snow decreases with the rise in air temperature. This results in water accumulating within the snowpack, and thus decreasing the scatter of light within the snowpack, lowering its surface albedo and attenuation coefficient (Mundy et al. 2005).

Throughout this transitional period (Phase I to II), ice algae are continually acclimating to their changing environment (Juhl & Krembs 2010); primarily, their biomolecular composition changes in response to light availability (Smith et al. 1987, Mock and Kroon 2002a, b, Leu et al. 2010, Pogorzelec et al. 2017). It is well known that algal cellular lipid production and storage is directly related to the amount of available light reaching the ice algal community (Mock and Kroon 2002b). The chloroplast, an important organelle within ice algal cells, is the site of cellular photosynthesis. It houses the thylakoid membrane, which is the site of photosynthetic pigments (i.e. Chl *a* and *b*, fucoxanthin, etc.) and the photosystems (I and II). Photosystems are responsible for converting light energy into chemical energy (generally stored as carbohydrates or sugars), which can then be utilized in the production of cellular lipids (Mock and Kroon 2002a, Campbell et al. 2008). Therefore, an increase in under-ice light availability will give rise to an increase in cellular lipid production and accumulation (i.e. storage lipids) and vice versa (Smith et al. 1987, Mock and Kroon 2002a, Leu et al. 2010). Additionally, it has been noted that photosynthetic pigments can be affected by the presence or absence of light; an increase in photoprotective pigments under thin snow cover, has been observed as an acclimation strategy against high light conditions (Alou-Font et al. 2013). However, this acclimation strategy is not rapid (dependent on algae's photo-acclimated state), as the sudden removal of snow can negatively impact the ice algae's net growth rate (i.e. increased cell death and decreased cell division; Juhl & Krembs 2010). By the end of Phase II, ice algae have accumulated a large

amount of saturated lipid (Leu et al. 2010) relative to protein content (nutrient dependent), which generally begins to decrease after Phase I (Mock and Kroon 2002a, b, Pogorzelec et al. 2017). Interestingly, unsaturated lipid (or PUFA) content also tends to decrease towards the end of Phase II (Leu et al. 2010).

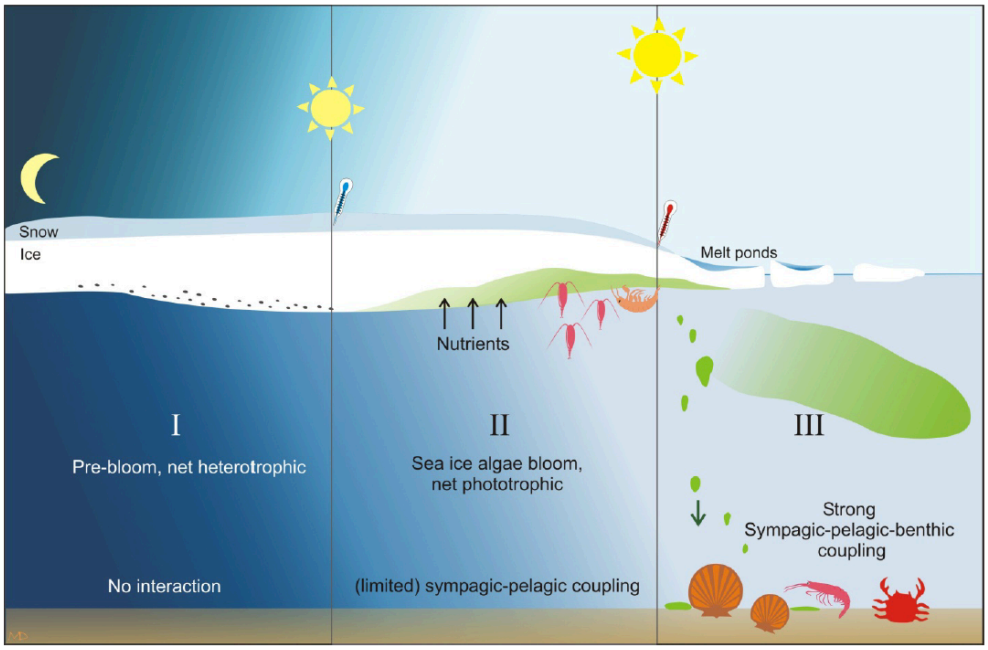


**Figure 2. 2:** Ice algal winter-spring bloom phase shift (Leu et al. 2015). Copyright © Elsevier (2015).

### *2.2.2 Nutrient Fluxes*

In the beginning of Phase II (Fig. 2.2), water column and in-ice nutrients are abundant and readily available to the ice algal community; however, near the end of Phase II, nutrients become limiting or are exhausted (Leu et al. 2015). As mentioned above, ice algae can inhabit different vertical horizons of the Arctic sea ice, with algae being most abundant in the bottom 0 to 10 cm of sea ice, due to ample nutrient supply and transport (Horner et al. 1992, Arrigo 2014, Leu et al. 2015). However, the mechanism by which nutrients are incorporated into sea ice is still relatively unknown. Several mechanisms for nutrient distribution have been proposed on the basis of

different studies of bottom ice algae. Meguro et al. (1967) reported ice algae 30 cm into the sea ice within the brine channels and pockets acclimating to their environment and actively growing. They proposed three plausible nutrient mechanisms; 1) recycled organic nutrients from biological and detritus pools (i.e. bacteria metabolic processes, decay of organisms, waste products, etc.), 2) forced water column penetration, and 3) brine drainage (considered to be the most important mechanism). Interestingly, Cota et al. (1987) came to a different conclusion and instead determined that water column mixing was required to meet the ice algal nutrient demand, instead of the mechanisms proposed by Meguro et al. (1967; mechanism 1 and 3). They proposed two possible routes for nutrient transport to the bottom ice algal community; 1) turbulent mixing of the upper water column as a result of shear instabilities associated with tidal currents along the ice bottom, also noting that fluctuations in tidal mixing could reflect fluctuations in ice algal biomass (nutrient pulses rather than a continuous flux of nutrients), and 2) convective mixing within the ice as a result of sea ice brine drainage. Smith et al. (1990) proposed that nutrients were likely algal-derived (high correlation between Chl *a* and dissolved nutrient concentration) and suggested that, after the initial uptake of nutrients from the water column, the algae would later serve as a nutrient reservoir, with the potential to release these nutrients during periods of osmotic stress (e.g., as what can occur during sample processing).

More recently, Dalman et al. (2019) reported a greater amount of ice algal biomass, both at the bottom and further up into the ice, towards the centre of a tidal strait near Cambridge Bay, NU. They proposed three mechanisms to explain enhanced ice algal production through nutrient replenishment in relation to increased currents along the tidal strait: 1) water column mixing, 2) enhanced molecular diffusion across the ice-ocean interface, and 3) forced convection within sea ice brine channels. The last of three proposed mechanisms is further examined in this thesis,

where the biomolecular composition of ice algae within the bottom fine (0-2, 2-5, and 5-10 cm) structure and bottom bulk (0-10 cm) structure of landfast sea ice across a tidal strait that was originally investigated by Dalman et al. (2019) will be examined (*see hypotheses 1-6*).

Nutrients (nitrate+nitrite, phosphate, and silicic acid) are a vital component of the spring ice algal bloom. As mentioned earlier, nutrients are abundant during the initial stages of Phase I and II (Gosselin et al. 1990, Smith et al. 1997, Leu et al. 2015) but diminish quickly as the ice algae begin to grow and divide (Figure 2.2), with nitrogen (specifically nitrate+nitrite) being the main limiting nutrient in the Arctic (Tremblay et al. 2015). This growth limiting nutrient can affect both cellular protein and lipid production. When nitrogen compounds are abundant, cellular protein production increases. In contrast, when nitrogen compounds are limiting and light availability is adequate, algae switch from protein to lipid production, via a change in cellular carbon allocation (Smith et al. 1997, Mock & Kroon 2002a, Pogorzelec et al. 2017).

By the end of Phase II, nutrients become depleted; this depletion signals the start of Phase III (post-bloom; Fig. 2.2), the gradual termination of the ice algal bloom and the beginning of the phytoplankton bloom. Phase III begins starts when daily temperatures are warm enough to begin the process of snow melt (evidence of melt ponds) and sea ice break-up (Leu et al. 2015).

## 2.3 FTIR SPECTROCHEMICAL IMAGING

The biochemical content of an individual diatom in natural (Giordano et al. 2001, Stehfast et al. 2005, Dean et al. 2010) and culture based (Heraud et al. 2008, Sackett et al. 2013, 2016) communities, as well as individually (Findley et al. 2015, Pogorzelec et al. 2017) is easily measured, using FTIR. FTIR samples can be imaged using three different imaging techniques viz., transmission, transflectance and attenuated total reflectance (ATR). In transmission, broad

band IR light passes through the sample, where some light is absorbed. The wavelengths of light that are absorbed match the vibrational energies of the molecular functional groups within the sample. The remaining light that is not absorbed continues to the detector and is recorded as an IR spectrum in percent transmittance. The spectrum is then converted into a plot of absorbance intensity (Abs=-log(%Transmittance)) versus wavenumber ($cm^{-1}$) (Griffiths & de Haseth 2007). In transflectance mode, the sample is mounted on an IR-reflective substrate. When IR light comes into contact with the sample, plus substrate, some of the light is absorbed. The remaining light is then reflected back and is captured by the detector, producing an IR spectrum. Lastly, in ATR, IR light passes through a crystal that is in direct contact with the sample. An evanescent wave is created that penetrates the sample by only few microns before passing back through the crystal. The light that was not completely absorbed is captured by the detector and an IR spectrum is produced (Griffiths & de Haseth 2007).

IR spectra present a record of molecular vibrational energy states ($E_{iv}$) that occur between molecules (i.e. a net change in dipole moment). This vibration follows the harmonic oscillation model (Figure 2.3). The model (following Hooke's law) describes the molecular stretching vibration, where the change in the potential energy between atoms results in the atoms' internuclear position (not mass) to change as well. For example, the change in internuclear position of atoms' in the diatomic molecule HCl (hydrochloric acid; Figure 2.4) during a stretching vibration. When energy (E) is applied, the internuclear separation (r) between hydrogen (H) and chlorine (Cl) results in the atoms to pull away for a short period of time (from $\nu = 0$ to $\nu = i$), before returning to their initial position ($\nu = 0$). Additionally, there are many other modes then stretching vibration, such as bending and twisting to name a few (Griffiths &

de Haseth 2007; page 4). The vibration energy states ($E_{iv}$) can be described by the following equation:

$$E_{iv} = h\nu_i(v_i + \frac{1}{2})$$

where, h is Plank's constant (J • s), $\nu_i$ is fundamental frequency of particular vibrational modes, and $v_i$ is the vibrational quantum number (Griffiths & de Haseth 2007).

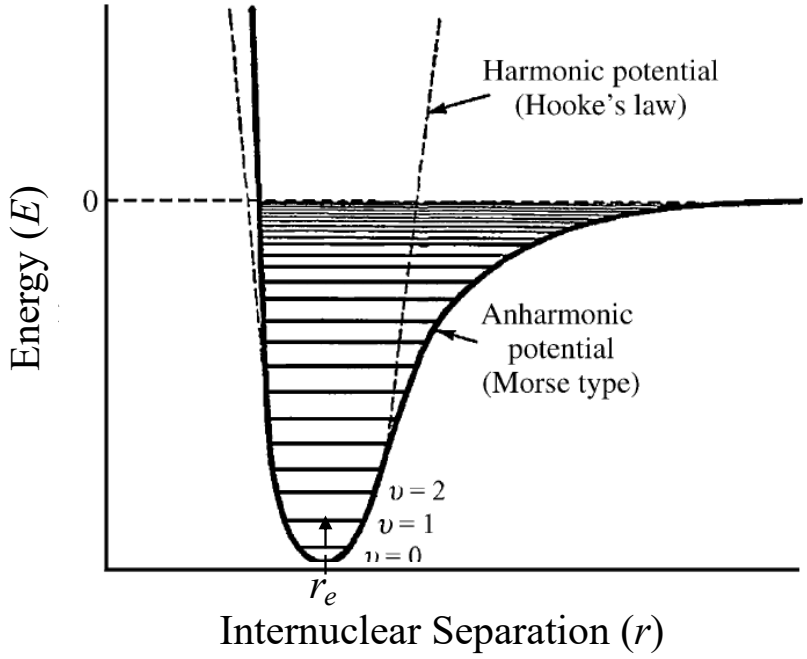


**Figure 2. 3:** The Harmonic oscillation model (dashed lines) for the energy (*E*) required to separate (*r*) a diatomic molecule (e.g. HCl). Modified Griffiths & de Haseth (2007) Figure 1.1; page 3. Copyright © John Wiley & Sons (2007).

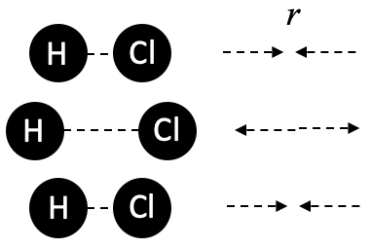


**Figure 2. 4:** An example of changing internuclear separation (r) separation during the H-Cl stretching vibration. Note: this is the only vibration for this molecule.

Additionally, the energy required to excite a particular molecular vibration is:

$$\Delta E = h\nu$$

where E is energy (J), h is Plank's constant (J • s) and ν is frequency of light (cm/s).

Furthermore,

$$\lambda\nu = c \quad \text{or} \quad \nu = \frac{c}{\lambda}$$

where λ is wavelength (cm), c is the speed of light (cm/s)

Therefore, energy can be written as:

$$\Delta E = h\left(\frac{c}{\lambda}\right) = hc\left(\frac{1}{\lambda}\right) = hc(\tilde{\nu})$$

where $(\tilde{\nu}) = \frac{1}{\lambda}(cm^{-1})$ is called a wavenumber (Griffiths & de Haseth 2007; page 4).

Following Beer's Law, the absorption of IR wavelengths can be described as:

$$A_i(\tilde{\nu}) = a_i(\tilde{\nu})bc_i$$

where $A_i(\tilde{\nu})$ is the absorption of species "i" to a specific wavenumber $(\tilde{\nu})$, $a_i(\tilde{\nu})$ is the species "i" ability to absorb at a specific wavenumber (concentration$^{-1}$ distance$^{-1}$), b is the path length, and $c_i$ is the concentration of species "i" (Griffiths & de Haseth 2007; page 13). The total transmittance (T) of IR wavelengths through a sample at a specific wavenumber $(\tilde{\nu})$, can be described as:

$$T(\tilde{\nu}) = \frac{I(\tilde{\nu})}{I_0(\tilde{\nu})} = \exp^{-\alpha(\tilde{\nu})b}$$

where $I(\tilde{\nu})/ I_0(\tilde{\nu})$ is the ratio that describes radiation passing through a sample (exit radiation/surface exposure radiation), $\alpha(\tilde{\nu})$ is the attenuation coefficient of species "i" at a specific wavenumber (cm$^{-1}$), and b is the path length (cm) or sample thickness the radiation must

travel (Griffiths & de Haseth 2007; page 12). The absorption of IR wavelengths by a sample ($A(\tilde{\nu})$) can then be described as:

$$A(\tilde{\nu}) = -\log_{10}\left(\frac{1}{T(\tilde{\nu})}\right) \text{ or } \log_{10}\left(\frac{1}{T(\tilde{\nu})}\right) = A_i(\tilde{\nu}) = \alpha_i(\tilde{\nu})bc_i$$

The absorbance intensities recorded for each functional group (a group of atoms in a molecule responsible for the given vibrational modes) represent the relative biomolecular content within any given cell. By using this technique, we can rapidly measure individual algal and community autecological responses to various environmental influences, such as the effect of light and nutrient stress on intracellular saturated and unsaturated lipid (PUFA), and protein content.

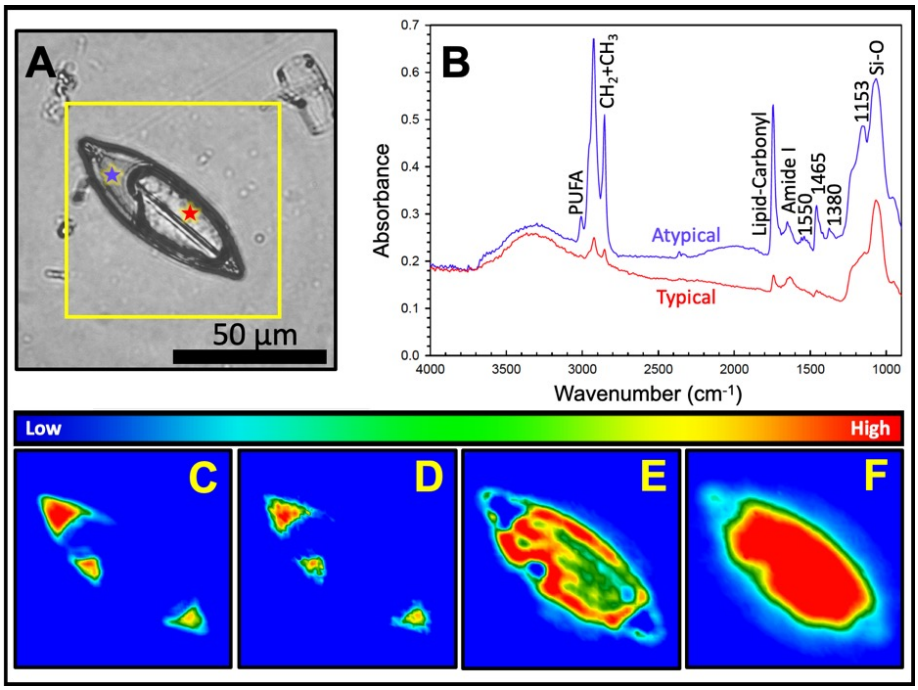


**Figure 2. 5:** A typical and atypical FTIR image of a diatom cell (*Navicula* spp.). (A) A visible light microscope image, (B) typical and atypical IR-spectrum, (C) saturated lipid ($CH_2$+$CH_3$), (D) PUFA, (E) protein (Amide I) and (F) biogenic silica (Si-O). Blue (atypical) and red (typical) stars indicate were spectrum were taken from diatom cell.

Various studies have used FTIR to evaluate biomolecular composition of both fresh water and marine algal species. However, only a handful of studies have exclusively examined the diatom class (Bacillariophyceae; Giordano et al. 2001, Stehfast et al. 2005, Heraud et al. 2008, Dean et al. 2010) and more rarely, polar marine diatoms (Sackett et al. 2013, 2016, Findley et al. 2015; Pogorzelec et al. 2017). Diatoms are known to exhibit strong IR band peaks (Fig. 2.5; Giordano et al. 2001, Stehfest et al. 2005, Sackett et al. 2014, Pogorzelec et al. 2017) associated with lipids ($CH_2$+$CH_3$; 3000 to 2800 $cm^{-1}$), proteins (Amide I, 1650 $cm^{-1}$ and Amide II, 1540 $cm^{-1}$), their silica frustule (Si-O stretching vibration; 1075 $cm^{-1}$), and carbohydrates (1200 to 900 $cm^{-1}$; generally obscured by Si-O), which was first reported by Giordano et al. (2001). As previously noted, the biomolecular composition of diatom cells can be greatly affected by environmental conditions, such as light and nutrient availability. Spectral bands associated with lipid ($CH_2$+$CH_3$) content are generally influenced by light availability, where an increase in available light increases cellular photosynthetic rates and in turn increases inorganic carbon assimilation and cellular lipid production (Mock and Kroon 2002a, b, Pogorzelec et al. 2017). Whereas, spectral bands associated with protein (Amide I and Amide II) tend to be lower in nutrient stressed diatoms, particularly nitrogen-starved diatoms (where N is $NH_4^+$, $NO_3^-$, and $NO_2^-$), and vice versa (Giordano et al. 2001, Stehfest et al. 2005, Pogorzelec et al. 2017). For example, Giordano et al. (2001) treated diatom cultures to two separate experimental conditions, namely nitrogen-starved, and nitrogen-enriched, over a one-week period. They observed a significant decrease in the diatom Amide I band, by about 50 to 60% after the first day under the nitrogen-starved conditions ($NH_4^+$ and $NO_3^-$; also observed in Stehfest et al. (2005) for nitrogen- and phosphorus-starved). An increase in the lipid ($CH_2$+$CH_3$) peak height was also observed in nitrogen-starved cells (Giordano et al. 2001, Stehfest et al. 2005, Pogorzelec et al. 2017),

attributed to an increase in carbon allocation towards lipid production (rather than protein production) as a cell stabilization mechanism (Mock and Kroon 2002a, b). The effect of nutrient limitation can also be observed in the lipid:protein ($CH_2$+$CH_3$:Amide I) and carbohydrate:protein (carbohydrate:Amide I) ratio (Stehfest et al. 2005, Dean et al. 2010, Pogorzelec et al. 2017), where a large ratio value is indicative of nutrient limitation versus a small ratio value, which suggests adequate nutrient availability. FTIR spectrochemical imaging has proven to be an efficient and sensitive technique in analysing the biomolecular composition in diatom cell.

# 2.5 REFERENCES


Ackley, S.F., Dieckmann, G., and Shen, H., (1987) Algal and form incorporation into new sea ice. EOS, 68: 1736

Ackley, S.F., and Sullivan, C.W., (1994) Physical controls on the development and characteristics of Antarctic sea ice biological communities-a review and synthesis. Deep Sea Research Part I: Oceanographic Research Papers, 41(10):1583-1604

Alou-Font, E., Mundy, C.J., Roy, S., Gosselin, M., and Agusti, S., (2013) Snow cover affects ice algal pigment composition in the coastal Arctic Ocean during spring. MEPS, 474:89-104

Arrigo, K.R., (2014) Sea ice ecosystems. Annu. Rev. Mar. Sci., 6:439-67. doi: 10.1146/annurev-marine-010213-135103

Arrigo, K.R., and Sullivan, C.W., (1992) The influence of salinity and temperature covariation on the photophysiological characteristics of Antarctic sea ice microalgae. J. Phycol., 28:746-756

Beattie, A., Hirst, E.L., and Percival, E., (1961) Studies on the metabolism of the Chrysophyceae. Biochem. J., 79:531-537

Campbell, K., Mundy, C.J., Landy, J.C., Delaforge, A., Michel, C. and Rysgaard, S. (2016) Community dynamics of bottom-ice algae in Dease Strait of the Canadian Arctic. Progress in oceanography, 149: 27-39

Campbell, N., Reece, J., (2008) Biology: Fifth Edn. Pearson Education. 1301 Sabsome St., San Francisco, CA 94111. ISBN-13: 978-0-8053-6844-4

Cota, G.F., (1985) Photoadaptation of high Arctic ice algae. Nature, 315(6016):219

Cota, G.F., Prinsenberg, S.J., Bennett, E.B., Loder, J.W., Lewis, M.R., Anning, J.L., Watson, N.H.F. and Harris, L.R., (1987) Nutrient fluxes during extended blooms of Arctic ice algae. Journal of Geophysical Research, 92: 1951-1962

Cox, G.F.N. and Weeks, W.F., (1988) Numerical simulations of the profile properties of undeformed first-year sea ice during the growth season. Geophysical Research, 93: 12,449-12,460

Crawford, R.M., (1981) Valve formation in diatoms and the fate of the silicalemma and plasmalemma. Protoplasma, 106:157-166

Dalman, L., Else, B., Williams, W.J., Carmack, E., Campbell, K., Barber, D., and Mundy, C.J., (2016) Enhanced ice algal biomass along tidal strait in the lower NW Passage of the Canadian Arctic. Arctic Net 2016 Poster Submission.

Dayton, P.K., Robilliard, G.A. and Devries, A.L., (1969) Anchor ice formation in McMurdo Sound, Antarctica, and its biological effects. Science, New Series, 163(3864):273-274

Dean AP, Sigee DC, Estrada B, Pittman JK (2010) Using FTIR spectroscopy for rapid determination of lipid accumulation in response to nitrogen limitation in freshwater microalgae. Bioresource Technol 101: 4499−4507

Fernández-Méndez, M., Olsen, L.M., Kauko, H.M., Meyer, A., Rösel, A., Merkouriadi, I., Mundy, C.J., Ehn, J.K., Johansson, A.M., Wagner, P.M. and Ervik, Å. (2018) Algal hot spots in a changing Arctic Ocean: sea-ice ridges and the snow-ice interface. Frontiers in Marine Science 5:75

Findlay, C., Morrison, J., Mundy, C.J., Sedlmair, J., Hirschmugl, C.J. and Gough, K.M., (2017) Thermal source Fourier transform infrared microtomography applied to Arctic sea ice diatoms. Analyst, 142(4):660-669

Garrison, D.L., Ackley, S.F. and Buck, K.R., (1983) A physical mechanism for establishing algal populations in frazil ice. Nature, 306(5941):363-365

Garrison, D.L. and Buck, K.R., (1986) Organism losses during ice melting: a serious bias in sea ice communities studies. Polar Biol 6:237-239

Garrison, D.L., Close, A.R. and Reimnitz, E., (1989) Algae concentrated by frazil ice: evidence from laboratory experiments and field measurements. Antarctic Science, 1(4):313-316

Giordano, M., Kansiz, M., Heraud, P., Beardall, J., Wood, B. and McNaughton, D., (2001) Fourier transform infrared spectroscopy as a novel tool to investigate changes in intracellular macromolecular pools in the marine diatom microalgae *Chaetoceros muellerii* (Bacillariophyceae). J. Phycol 37: 271-279.

Gosselin, M., Legendre, L., Therriault, J.C. and Demers, S., (1990) Light and nutrient limitation of sea-ice microalgae (Hundson Bay, Canadian Arctic). J. PhycoL, 26:220-232

Gosselin, M., Legendre, L., Therriault, J.C. and Demers, S., (1997) New measurements of phytoplankton and ice alga production in the Arctic Ocean. Deep-Sea Research Ii, 44(8):1623-1644

Griffiths, P., and de Haseth, J., (2007) Fourier Transform Infrared Spectroscopy, 2nd edn. John Wiley & Sons, New Jersey

Gradinger, R., (1999) Vertical fine structure of the biomass and composition of algal communities in Arctic pack ice. Marine Biology, 133:745-754

Gradinger, R. and Ikävalko, J., (1998) Organism incorporation into newly forming Arctic sea ice in the Greenland Sea. Journal of Plankton Research, 20(5):871-886.

Heraud, P., Wood, B.R., Beardall, J. and McNaughton, D., (2007) Probing the Influence of the Environment on Microalgae Using Infrared and Raman Spectroscopy. New Approaches in Biomedical Spectroscopy. American Chemical Society, Washington, DC, 85-106

Horner, R., Ackley, S.F., Dieckmann, G.S., Gulliksen, B., Hoshiai, T., Legendre, L., Melnikov, I.A., Reeburgh, W.S., Spindler, M. and Sullivan, C.W., (1992) Ecology of sea ice biota: 1. Habitat, terminology, and methodology. Polar Biol, 12:417-427

Horner, R. and Schrader, G.C (1982) Relative contributions of ice algae, phytoplankton, and benthic microalgae to primary production in nearshore regions of the Beaufort Sea. Arctic, 485-503

Juhl, A.R. and Krembs, C., (2010) Effects of snow removal and algal photacclimation on growth and export of ice algae. Polar Biol, 33:1057-1065

Kröger, N., (2007) Prescribing diatom morphology: toward genetic engineering of biological nanomaterials. Current Opinion in Chemical Biology, 1:662-669

Leu, E., Wiktor, J., Søreide, J.E., Berge, J. and Falk-Petersen, S., (2010) Increased irradiance reduces food quality of sea ice algae. Marine Ecology Progress Series, 411:49-60

Leu, E., Mundy, C.J., Assmy, P., Campbell, K., Gabrielsen, T.M., Gosselin, M., Juul-Pedersen, T. and Gradinger, R., (2015) Arctic spring awakening-steering principles behind the phenology of vernal ice algae blooms. Progress in Oceanography, 139:151-170

Olsen, L.M., Laney, S.R., Duarte, P., Kauko, H.M., Fernández-Méndez, M., Mundy, C.J., Rösel, A., Meyer, A., Itkin, P., Cohen, L. and Peeken, I., (2017). The seeding of ice-algal blooms in Arctic pack ice: the multiyear ice seed repository hypothesis. Journal of Geophysical Research: Biogeosciences. doi**:** 10.1002/2016JG003668

McMinn, A., and Hegseth, E.N., (2004) Quantum yield and photosynthetic parameters of marine microalgae from the southern Arctic Ocean. Svalbard. Journal of the Marine Biological Association of the United Kingdom, 84(5):865-871.

Meguro, H., Ito, K. and Fukushima, H., (1967) Ice flora (bottom type): a mechanism of primary production in polar seas and the growth of diatoms in sea ice. Arctic, 114-133.

Mock, T. and Gradinger, R. (1999) Determination of Arctic ice algal production with a new in situ incubation technique. Marine Ecology Progress Series, 177:15-26

Mock, T., and Kroon B., (2002a) Photosynthetic energy conversion under extreme conditions-I: important role of lipids as structural modulators and energy sink under N-limited growth in Antarctic sea ice diatoms. Phytochemistry, 61:41-51

Mock, T., and Kroon, B., (2002b) Photosynthetic energy conversion under extreme conditions-II: the significant of lipids under light limited growth in Antarctic sea ice diatoms. Phytochemistry, 61:53-60

Mundy, C.J., Barber, D.G. and Michel, C., (2005) Variability of snow and ice thermal, physical and optical properties pertinent to sea ice algae biomass during spring. Journal of Marine Systems, 58:107-120

Niemi, A., Michel, C., Hille, K. and Poulin, M., (2011) Protist assemblages in winter sea ice: setting the stage for the spring ice algal bloom. Polar Biology 34:1803-1817

Perovich, D.K., Roesler, C.S. and Pegau, W.S., (1998) Variability in Arctic sea ice optical properties. Journal of Geophysical Research 103:1193-1208

Pogorzelec, N.M., Mundy, C.J., Findlay, C.R., Campbell, K., Diaz, A., Ehn, J.K., Rysgaard, S. and Gough, K.M., (2017) FTIR imaging analysis of cell content in sea-ice diatom taxa during a spring bloom in the lower Northwest Passage of the Canadian Arctic**.** MEPS, 69:77-88

Poulin, M., Daubjerg, N., Gradinger, R., Ilyash, L., Ratkova, T., and von Quillfedt, C., (2011) The pan-Arctic biodiversity of marine pelagic and sea-ice unicellular eukaryotes: a first-attempt assessment. Mar. Biodiv., 41:13-28

Rózańska, M., Gosselin, M., Poulin, M., Wiktor, J.M. and Michel, C. (2009) Influence of environmental factors on the development of bottom ice protist communities during the winter–spring transition. Marine Ecology Progress Series, 386:43-59

Round, F., Crawford, R., and Mann, D., (1990) Diatoms: biology and morphology of the genera. Cambridge University Press.

Sackett O, Petrou K, Reedy B, De Grazia A, Hill R et al. (2013) Phenotypic plasticity of Southern Ocean diatoms: key to success in the sea ice habitat? PLoS ONE 8(11): e81/85. doi:10.137/journal.pone.j081185

Sackett, O., Petrou, K., Reedy, B., De Grazia, A., Hill, R., Doblin, M., Beardall, J., Ralph, P. and Heraud, P., (2014) Taxon-specific responses of Southern Ocean diatoms to Fe enrichment reveale by synchrotron radiation FTIR microscopy. Biogeoscience, 11:5795-5808.

Sackett, O., Petrou, K., Reedy, B., Hill, R., Doblin, M., Beardall, J., Ralph, P. and Heraud, P., (2016) Snapshot prediction of carbon productivity, carbon and protein content in Southern Ocean diatom using FTIR spectroscopy. The ISME Journal 10:416-426

Stehfest, K., Toepel, J. and Wilhelm, C., (2005) The application of micro-FTIR spectroscopy to analyse nutrient stress-related changes I biomass composition of phytoplankton algae. Plant Physiol Bioch 43: 717-726

Smith, R.E., Clement, P., Cota, G.F. and Li, W.K., (1987) Intracellular photosynthate allocation and the control of arctic marine ice algal production. Journal of Phycology, 23(2):124-132

Smith, R.E., Harrison, W.G., Harris, L.R. and Herman, A.W., (1990) Vertical fine structures of particulate matter and nutrients in sea ice of the high Arctic. CAN J. FISH. AQUAT. Sci, 47:1348-3155

Smith, R.E.H., Gosselin, M. and Taguchi, S., (1997) The influence of major inorganic nutrients on the growth and physiology of high arctic ice algae. Journal of Marine Systems 11:63-70

Spindler, M., (1994) Notes on the biology of sea ice in the Arctic and Antarctic. Polar Biol, 14:319-324

Syvertsen, E.E., (1991) Ice algae in the Barent Sea: types of assemblages, origin, fate and role in the ice-edge phytoplankton bloom. Polar Research, 10(1):277-288

Weissenberger, J. and Grossmann, S., (1998) Experimental formation of sea ice: importance of water circulation and wave action for incorporation of phytoplankton and bacteria. Polar Biol, 20:178-188.

# CHAPTER 3: FTIR AUTECOLOGICAL ANALYSIS OF BOTTOM-ICE DIATOM TAXA ACROSS NUTRIENT GRADIENTS IN A TIDAL STRAIT, CANADIAN ARCTIC

This manuscript has been prepared for submission to the Journal of *Elementa: Science of the Anthropocene*. The work detailed here represents a central chapter of my thesis and, therefore, as first author the work was conducted, analysed, and reported by myself.

Pogorzelec, N.M., Gough, K.M., Ha, S., Campbell, K., Else, B., and Mundy, C.J. FTIR autecological analysis of bottom-ice diatom taxa across nutrient gradients in a tidal strait, Canadian Arctic. Elementa: Science of the Anthropocene (*in progress*).

## 3.1 ABSTRACT

A recent study demonstrated that tidal straits, where shoaled and constricted waterways increase tidally driven sub-ice currents and turbulence, represent ice algal production hotspots due to a hypothesized enhanced ocean-ice nutrient supply. Based on these findings, we sampled the bottom ice algal community across the same tidal strait between the Finlayson Islands within Dease Strait, NU, Canada in spring 2017. Our objective was to examine sea ice diatom cellular responses to two expected nutrient supply gradients in their natural environment: (1) a spatial gradient across the tidal strait and (2) a vertical gradient up into the bottom ice matrix. Two diatom taxa, *Nitzschia frigida* and *Attheya* spp. within the bottom ice sections (0-2, 2-5, and 5-10 cm) under thin snow cover (<5 cm) were selected for Fourier Transform Infrared (FTIR) spectrochemical analysis for lipid and protein content. Results from the FTIR technique strongly supported the existence of a spatial nutrient gradient across the tidal strait of the Finlayson Islands, while particulate organic carbon (POC) and chlorophyll *a* (Chl *a*) concentration estimates were difficult to interpret. Spatially, the larger *N. frigida* cells appeared to be more

sensitive to the nutrient gradient, significantly increasing (decreasing) in lipid (protein) content towards the outside of the tidal strait. In contrast, the epiphytic diatom, *Attheya* spp., was more sensitive to the vertical gradient, where above 2 cm into the bottom-ice matrix, the non-motile cells were trapped with a depleted nutrient inventory with evidence of a post-bloom state. Application of the FTIR technique to estimate algal cell biomass composition provided new insights on the response of the bottom ice algal community to the examined nutrient supply gradients that could not be attained from conventional bulk measurements alone. Therefore, future studies are encouraged to employ the use of this technique.

## 3.2 INTRODUCTION

Ice algae play a significant role as the main primary producer during early spring, synthesizing high-energy essential fats that sustain the Arctic marine food-web (Smith et al. 1987, Mock & Gradinger 2000, Mock & Thomas 2005, Leu et al. 2010, Søreide et al. 2010). The bottom-ice algal community inhabits the bottommost layers of the Arctic sea ice (0-10 cm; Horner et al. 1992, Arrigo 2014, Leu et al. 2015), with diatoms being the dominant taxa during the spring bloom (Różańska et al. 2009, Poulin et al. 2010, van Leeuwe et al. 2018). The bloom of sea ice diatoms begins under low-light and nutrient replete conditions during late winter to early spring (Poulin et al. 2010). However, the rise in average global temperatures has resulted in a decline in sea ice extent and thickness, caused by later freeze-up and longer melt period (Comiso et al. 2008, Markus et al. 2009, Stroeve et al. 2012). This rapid change will likely have a strong effect on the phenology and contribution of ice algae to total production (Leu et al. 2015, Tedesco et al. 2019) with the potential of a cascading effect on the Arctic marine food-web (Michel et al. 2006, Søreide et al. 2010).

Under-ice photosynthetically active radiation (PAR) is limited by sea ice thickness and more importantly, by the high albedo and strong attenuation properties of the overlying snow cover (Perovich et al. 1998, Perovich 2018). As a result, spring ice algal biomass often has a significant negative relationship with snow depth (Campbell et al. 2016). However, during their spring bloom, ice algae experience a transition from initial light limitation to nutrient limitation, as light increases and algal growth demand exceeds available nutrients in the sea ice matrix (Cota et al. 1987).

The main nutrient supply to the ice algal community is from the underlying water column and across the ocean-ice boundary layer (Gosselin et al. 1985; Cota et al. 1987; Dalman et al. 2019). A strong temperature gradient in the ice bottom from the warm ocean to cold atmosphere in winter/spring reduces brine volume space, thereby reducing convection higher into the ice matrix (Vancoppenolle et al. 2013). Therefore, it is expected that nutrient supply to the ice algal community decreases with distance from the ocean-ice interface. Spatially, Dalman et al. (2019) concluded that tidal straits (shoaled and constricted waterways dominated by tidal current flow) represent localized hotspots of ice algal production. This conclusion was derived from observations of increased tidally driven currents and mixing, reduced stratification, and greater ice algal biomass towards the centre of a tidal strait. Therefore, it is expected that the greater currents towards the centre of a tidal strait provide an enhanced ocean-ice nutrient flux to the bottom-ice algal.

Lipid and protein content of individual diatoms is dependent on light and nutrient availability. An increase in PAR results in an increase in cellular photosynthetic rate and lipid production, while a decrease in nutrient (i.e. nitrate and nitrite) availability has been shown to result in increased lipid storage and a decreased protein production, i.e. redirection of assimilated

carbon (Mock & Kroon 2002a, b, Pogorzelec et al. 2017). Fourier Transform Infrared (FTIR) spectrochemical analysis is efficient in measuring the relative abundance of cellular lipid ($CH_2$+$CH_3$) and protein (Amide I) content, as well as individual diatom cells response to light and nutrient stress (Giordano et al. 2001, Stehfast et al. 2005, Stackett et al. 2014 & 2016, Pogorzelec et al. 2017). In this study, we used FTIR spectrochemical imaging to assess the biomolecular composition of individual diatom cells in response to the two aforementioned nutrient supply gradients: (1) a vertical gradient in the bottom-ice matrix over 0-2, 2-5, and 5-10 cm sections, and (2) a spatial gradient across a tidal strait.

The Kitikmeot Sea in the western Canadian Arctic is a highly nitrogen-depleted system (Campbell et al. 2017, Pogorzelec et al. 2017), creating a logical location for the examination of nutrient gradient impacts on a natural ice algal community (Dalman et al. 2019). We hypothesize that greater nutrient supply occurs in the bottommost ice sections and at the centre of the tidal strait, resulting in detectable increases in protein production and decreases in lipid storage. Samples were collected over a 2-week period between April and May during the 2017 Ice Covered Ecosystem-Cambridge Bay Process Study (ICE-CAMPS) campaign. Contrasting responses in biomolecular composition were observed for two diatom taxa, *Nitzschia frigida* (pennate) and *Attheya* spp. (centric), with implications for species succession in the system.

# 3.3 MATERIALS AND METHODS

## 3.3.1 Field Collection

Samples were collected once every three days during the 2017 ICE-CAMPS field campaign, between 26 April and 12 May. The field site was located on landfast sea ice within a tidal strait area between the Finlayson Islands (~69˚00.033’N, 105˚48.967’W), in the Kitikmeot Sea,

Nunavut, Canada. The four sample sites (Fig. 3.1) were spaced along a transect from within (sites 1 and 2) and outside (sites 3 and 4) the tidal strait, in order to access variation in under-ice currents and water column mixing. At each site, four ice cores were collected under thin snow cover (<5 cm depth) using a 9-cm inner diameter Mark II Coring System (Kovacs Enterprises). After extraction, ice cores were kept shaded to minimize potential changes to the biomolecular composition of the ice algae (Leu et al. 2010, Stitt et al. 2012). The bottom 10 cm length of each core was segmented into ice sections of 0-2, 2-5, and 5-10 cm for diatom collection. An additional 10 cm bottom ice core was collected and sectioned into 0-2, 2-5, and 5-10 cm ice sections, for measurements of salinity (Thermo Scientific - ORION STAR A212) and nutrients (i.e. phosphates, nitrate+nitrite, silicic acid).

Core segments for particulate analysis were pooled in the dark within insulated containers for transport and melting. Filtered seawater (FSW; 0.2 μm membrane filter) was added to the containers at a 3:1 ratio (FSW:pooled ice cores) and left overnight to melt. The FSW was added to minimize osmotic stress on diatoms during sea ice melt (Garrison & Buck 1986, Rintala et al. 2014, Campbell et al. 2018).

Several environmental measurements were collected in conjunction with ice core collection, including snow depth, ice thickness, and spectral downwelling irradiance, albedo (upwelling:downwelling irradiance), and under-ice PAR transmittance irradiance. The spectral irradiance was measured with a hyperspectral radiometer (Satlantic HyperOCR) calibrated for air and water immersion. An articulating arm was used to position the sensor in the air at the surface to make measurements of downwelling and upwelling irradiance and downwelling irradiance in the water immediately below the ice cover.

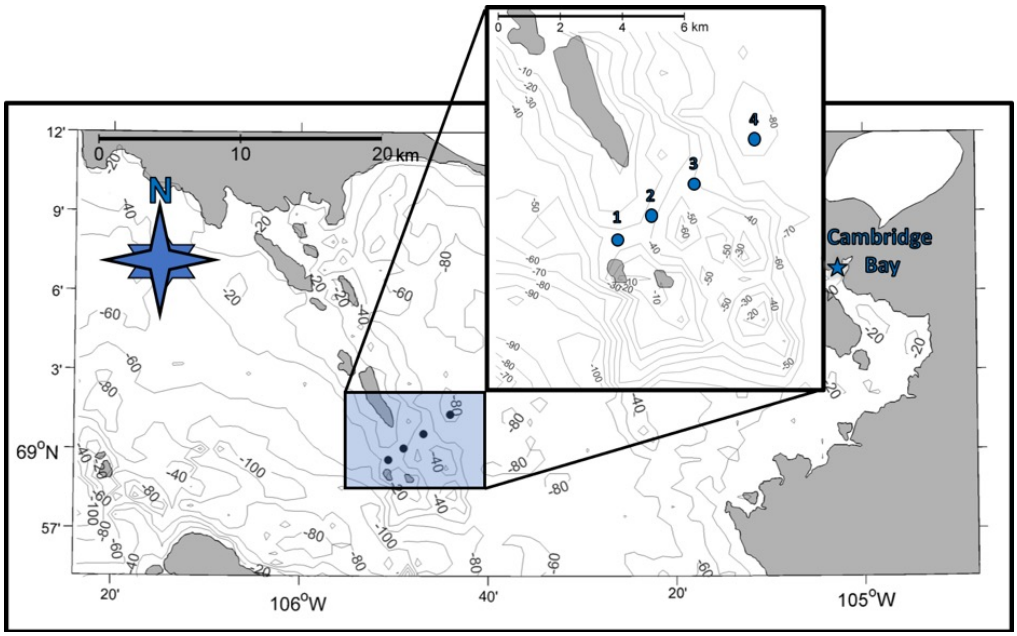


**Figure 3. 1:** Map of field site locations between the Finlayson Island, near Cambridge Bay, NU, CA. Site locations (1 through 4) are highlighted in blue with a magnified version located in the top right corner.

### 3.3.2 Bulk Community Sample Collection & Nutrient Analysis

Ice core layers for dissolved nutrient concentration analysis were melted in the dark without FSW and in a sterile Whirlpak bag. The ice melt was filtered through an acid-washed (10% HCl) swinnex-filter with a GF/F filter, pre-combusted at 450˚C for 5 h, and stored in an acid-washed 15-ml falcon tube at -20˚C, until analysis at the Université du Québec à Rimouski. Concentrations of phosphate, nitrate+nitrite, and silicic acid were determined with a Seal Analytical Auto-Analyzer 3 as described in Grasshoff et al. (1999).

Taxonomy samples were prepared by combining 100 ml of FSW-diluted ice core melt and 4 ml of Lugol's Acid in a 125 ml amber glass bottle, which was stored at 4˚C. Diatom taxonomic surveys and cell counts for target species, total pennate and centric diatoms, and other ice algal taxa (i.e., flagellate, dinoflagellate, and unknown) were accomplished with an inverted light

microscope and Ütermohl type chamber (i.e. Hydrobios method; Lund et al. 1958, Campbell et al. 2018).

Samples for measurement of particulate organic carbon (POC) were collected by filtration of 200 to 400 ml of FSW-diluted ice core melt in indirect light conditions onto a GF/F filter pre-combusted at 450˚C for 5 h, wrapped in a pre-combusted aluminium casing and stored at -80˚C. Samples were analyzed for POC concentration within 3 months using an Elemental Analyzer (Elementar Vario Micro Cube) as described in Cutter et al. (2014).

For chlorophyll a (Chl *a*) determination, 5 to 200 ml of FSW-diluted ice core melt was filtered onto a 25 mm GF/F filter and stored at -80˚C. The Chl *a* pigment was extracted from the filter by adding 10 ml of 90% acetone and storing the filter in the dark at 4˚C for 18 h before analysis. Chlorophyll *a* fluorescence was measured before and after acidification with 5% HCl (Parsons et al. 1984), using a Turner Designs Trilogy Fluorometer and converted into Chl *a* concentration (mg $m^{-2}$) according to the equations described in Holm-Hansen et al. (1965).

### 3.3.3 Sample Preparation & FTIR Analysis

All procedures were conducted in a darkened environment to prevent photo-oxidation of cellular fatty acids (Sattar et al. 1976, Stitt et al. 2012). Diatoms had been collected by filtering 5 to 200 ml FSW-diluted ice core melt onto a 5-µm pore size polycarbonate membrane filter (SterliTech Corp. USA). The filter was folded in half, wrapped in an aluminum casing and stored at -80°C until analysis, within 2 months. Diatom cells were transferred onto a 25-mm diameter, 2-mm thick barium fluoride ($BaF_2$) substrate by pipetting a 4-µl ultra-pure (Milli-Q) droplet on the substrate and placing a segment of the polycarbonate filter onto the droplet. The filter was gently agitated against the droplet to release the diatoms and left to settle for approximately 1 min. Excess water was wicked away with a tissue (Kim-Wipe). A compound light microscope

equipped with a 650-nm red photo light filter (to prevent photo-oxidization of lipids; Sattar et al. 1976, Stitt et al. 2012), was used to identify and select individual diatom cells on the $BaF_2$ substrate. Substrates were placed in a desiccant chamber and in the dark with silica beads overnight.

Two dominant diatom taxa were targeted to obtain a range of cell size (Poulin et al. 2011, Campbell et al. 2018, van Leeuwe et al. 2018). These included one pennate diatom, *Nitzschia frigida* (average cell size of 68 x 8 µm; Fig. 3.2) and one epiphytic centric diatom, *Attheya* spp. (average cell size of 9 x 10 µm, without setae).

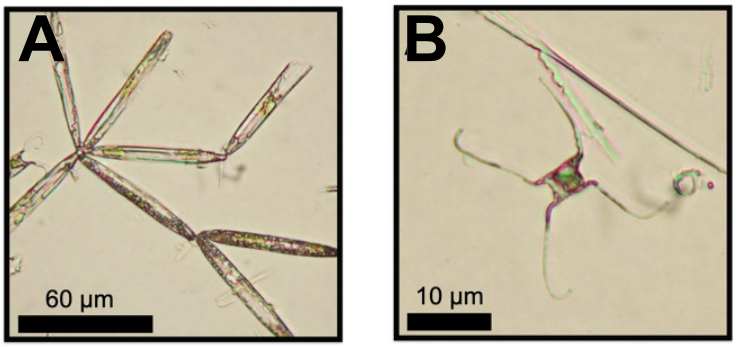


**Figure 3. 2:** Light microscopic images of the targeted FTIR diatom taxa: (A) *Nitzschia frigida* and (B) *Attheya* spp.

Approximately 18 h after sample preparation, individual diatoms were scanned with an Agilent Cary 670 Fourier Transform Infrared (FTIR) spectrometer coupled to a 620 IR imaging microscope in transmission mode (Pogorzelec et al. 2017). The IR microscope was equipped with a 15$x$ objective and condenser, a numerical aperture (NA) of 0.62, and a 64 $x$ 64 Focal Plane Array (FPA) detector that resulted in a spatial resolution of 1.1 $x$ 1.1 $\mu m^2$ pixel dimension (Findlay et al. 2015; Pogorzelec et al. 2017). All spectra were recorded at 8 $cm^{-1}$ spectral resolution and a zero-fill factor of 2, with co-additions of 512 scans for the background and 256 scans for sample. Spectra and false coloured images were initially processed for diatom biomolecular content in Resolutions Pro™ (version 5.2.0, Agilent Technologies Inc.; Pogorzelec

et al. 2017). The images were exported to MATLAB$^{TM}$ for further processing as detailed elsewhere (Findlay et al. 2015; Pogorzelec et al. 2017).

### 3.3.4 Statistical Analysis

Linear regression analyses were conducted to examine spatial differences in variables across the tidal strait. Spatial linear regressions were only performed on data from the 0-2 cm ice sections, under the assumption that this layer was most directly influenced by ocean-ice fluxes. In contrast, vertical ice sections were tested for differences using a two factor repeated measures ANOVA (one-way ANOVA for cell count; F-statistic; $\alpha = 0.05$). The repeated measures ANOVA was used to remove spatial trends from the analysis. Prior to the ANOVA tests, data were tested for normality using a Shapiro-Wilk test. If the Shapiro-Wilk test failed, a Kruskal-Wallis one-way ANOVA on ranks test (H-statistic) was used to test for significant differences between vertical ice sections. If the ANOVA was found to be significant a Tukey's post hoc test was conducted to determine differences between ice section pairs.

## 3.4 RESULTS

### 3.4.1 Physical & Chemical Environmental Conditions

Snow depth significantly decreased from site 1 to site 4, while ice thickness significantly increased (Fig. 3.3A). PAR albedo was consistent across sites, whereas percent PAR transmittance slightly increased from roughly 2 to 2.5% from sites 1 to 4 where snow depth was lowest at site 4 (Fig. 3.3B). However, PAR transmittance was not significantly different across sites.

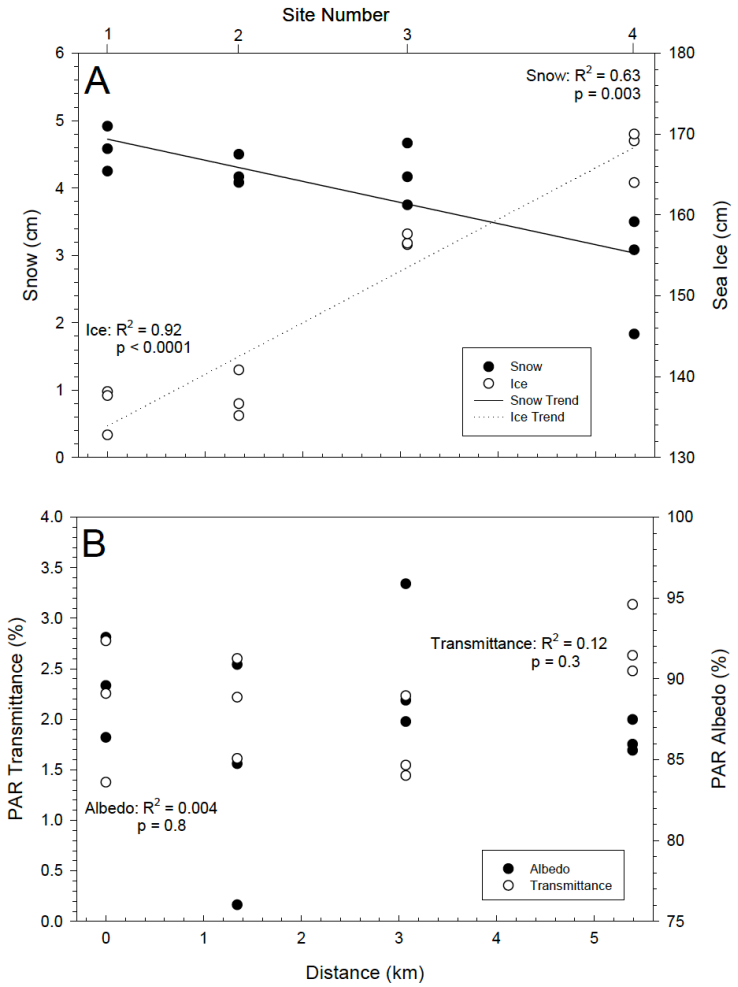


**Figure 3. 3:** Environmental conditions across sites (1, 2, 3, and 4) for (A) snow depth ($y = 4.73 - 0.31x$ ) and sea ice thickness ($y = 133.9 + 6.4x$), and (B) percent transmittance and percent albedo. Lines represent significant linear trends.

No significant relationships were observed for distance from the tidal strait (site 1) versus outside for salinity, phosphate and nitrate+nitrite (Fig. 3.4A-C). Bottom ice salinity and nutrient concentrations were significantly greater in the bottom 0-2 cm ice section (Sup. Table 3.1). Averaged phosphate, nitrate+nitrite, and silicic acid concentrations for 0-2 to 5-10 cm ranged from 5 ± 2 to 0.2 ± 0.06, 2 ± 0.9 to 0.4 ± 0.2, and 5 ± 2 to 0.9 ± 0.5 μmol $L^{-1}$, respectively (Fig. 3.4B-D; Sup. Table 3.1).

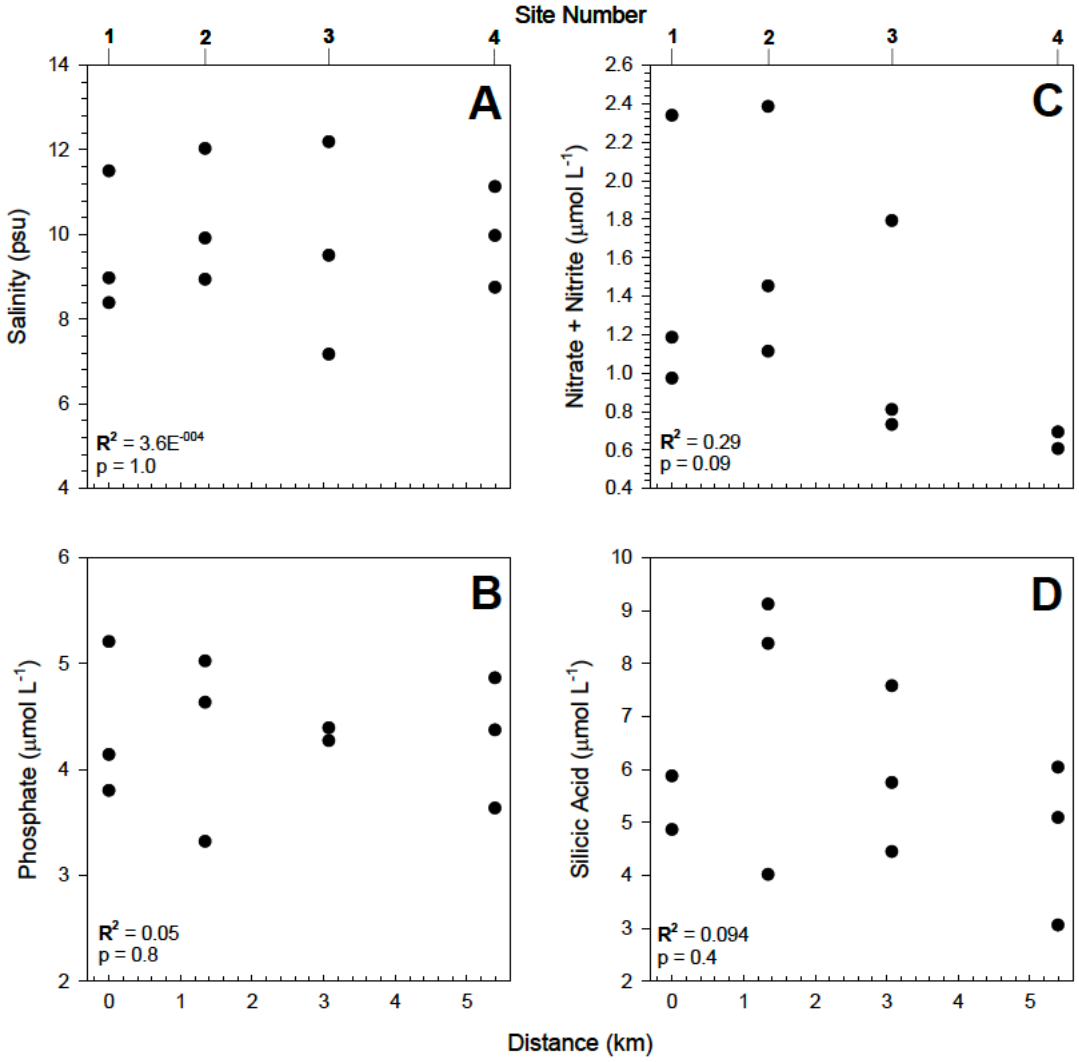


**Figure 3. 4:** (A) Salinity and dissolved inorganic nutrient concentrations within 0-2 cm sea layer per site for (B) phosphate, (C) nitrate+nitrite, and (D) silicic acid.

### 3.4.2 Ice algal Community

Diatoms dominated the ice algal community; pennate and centric diatoms accounted for more than 80% of the population (Fig. 3.5A-C). Relative abundance of other ice algal taxa (i.e., flagellate, dinoflagellate and unidentified taxa) noticeably increased above the 0-2 cm ice section (Fig. 3.5C), with the 2-5 and 5-10 cm section having relatively equal proportions (Fig. 3.5A-B).

Enumeration of intact diatom cells and empty frustules showed that the relative contribution of intact centric cells slightly increased up into the sea ice matrix (13-20% to 18-27%), whereas that of pennates strongly decreased (65-85% to 16-29%; Fig. 3.5D-F). Interestingly, the relative abundance of empty pennate frustules increased from the 0-2 cm section (6-18%; Fig. 3.5F) towards the 5-10 cm ice section (43-61%; Fig. 3.5D). Empty centric frustules, however, did not greatly increase in relative abundance (0.6–2% to 2–5%).

Of the two diatom species targeted for FTIR analysis (Fig. 3.5G-I), *Attheya* spp. dominated the centric community with the greatest cell abundance (13.4 to 50%), especially further away from the ocean-ice interface. While, *N. frigida* relative abundance noticeably decreased from 12-25 % at the 0-2 cm ice section to 0.2-4% (5-10 cm). Both species significantly decreased in total abundance up into the ice matrix (Table 3.1). Interestingly, *Attheya* spp. exhibited epiphytic associations with pennate diatom cells only in the 0-2 cm ice section, while cells were always observed as solitary in the 2-5 and 5-10 cm ice sections.

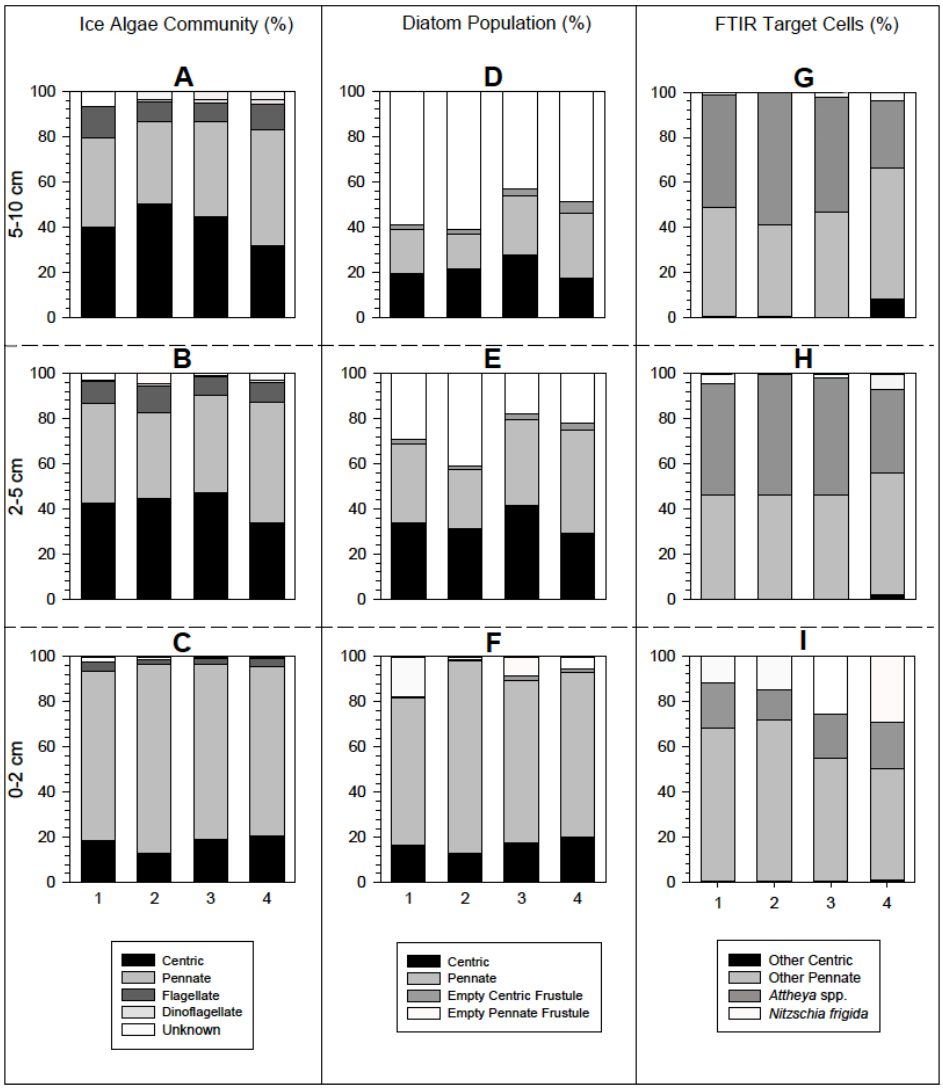


**Figure 3. 5:** Relative community composition of ice algal taxa within sea ice sections (A) 5-10 cm, (B) 2-5 cm, and (C) 0-2 cm; relative proportion of diatom intact cells and empty frustules for ice sections (D) 5-10 cm, (E) 2-5 cm, and (F) 0-2 cm; and relative contribution of targeted FTIR diatoms to the intact-cell diatom population for ice sections (G) 5-10 cm, (H) 2-5 cm, and (I) 0-2 cm.

Particulate organic carbon (POC) was significantly greater in the 0-2 cm ice section (Fig. 3.6A; Table 3.1), with an average value of 500 ± 170 mg $m^{-2}$ across all sites. In fact, all bulk measurements (i.e. POC, Chl *a* and POC:Chl *a*) were found to be significantly different vertically (tow factor repeated measures ANOVA $p < 0.01$) between most ice sections (Table 3.1). However, POC in the 0-2 cm ice section did not exhibit a significant spatial relationship. In

contrast, the 0-2 cm ice section for Chl *a* concentration was observed to follow a significant decreasing trend further away from the tidal strait (Fig. 3.6B; Table 3.1), ranging from of 9.3 ± 2 at site 1 to 4.1 ± 1.3 mg $m^{-2}$ at site 4. The POC:Chl *a* ratio (Fig. 3.6C) increased spatially from site 1 to site 4; however, this increase was not significant (Table 3.1).

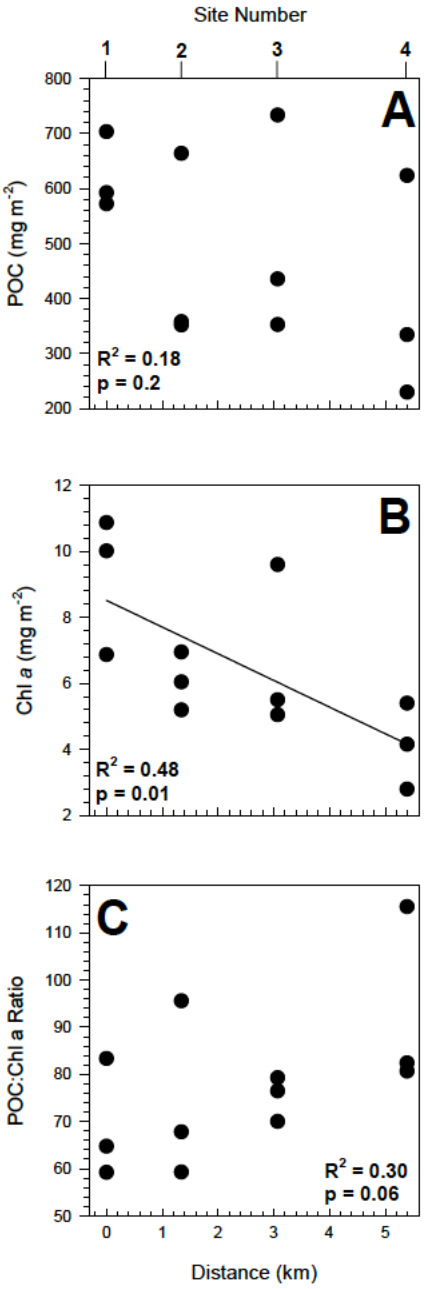


**Figure 3.6:** Bulk ice algal community biomass measurements within 0-2 cm of sea ice per site for (A) POC, (B) Chl *a* ($y = 8.52 - 0.81x$), and (C) POC:Chl *a* ratio. Solid line represents significant linear trend.

### 3.4.3 Cellular biomass composition

#### *3.4.3.1 Typical Diatom FTIR Spectrum*

Spectra and false-coloured images of two separate pixels within a diatom cell (e.g. *N. frigida*) is shown in Figure 3.7. Spectra were processed for lipid content (integrated asymmetric and symmetric $CH_2$+$CH_3$ bands: between 2969 and 2840 $cm^{-1}$), protein (Amide I: 1645 $cm^{-1}$), and silica (Si-O: 1075 $cm^{-1}$) content. Two selected pixel-points show the typical variation in IR spectra within a single diatom, i.e., within a chloroplast area (blue) and outside the chloroplast (red). Cellular saturated lipid and protein content are observed to be greatest in the chloroplast region of the cell (red spectrum) versus areas found just outside the chloroplast (blue spectrum).

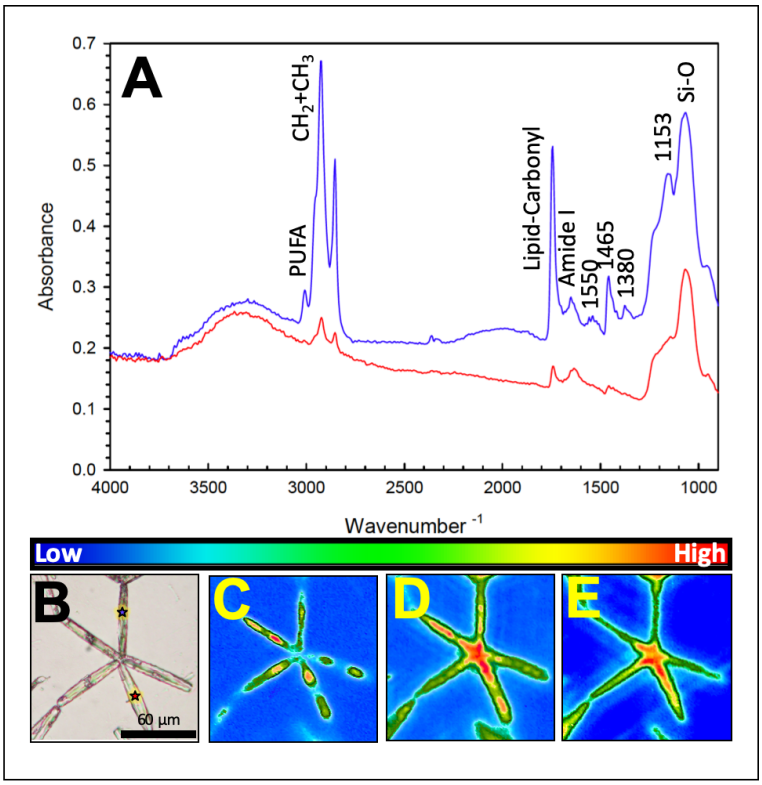


**Figure 3. 7:** FTIR spectra of a typical diatom (*N. frigida*.) with false colour images. (A) Red and blue diatom IR spectrum, (B) light microscopic image of *N. frigida* with red and blue stars, (C) integrated saturated $CH_2$+$CH_3$ (lipid), (D) Amide I (protein), and (E) Si-O (silica).

*3.4.3.2 Nitzschia frigida* & *Attheya* spp.

*Nitzschia frigida* cellular saturated lipid content per pixel significantly increased towards the outside of the tidal strait (site 4) for the 0-2 cm section (Fig. 3.8A). Vertically, no significant difference in lipid content between ice sections was observed (Table 3.1). *Attheya* spp. averaged saturated lipid content was observed to be the lowest in the 0-2 cm ice section (Fig. 3.8B), versus that of the 2-5 and 5-10 cm layer. *Attheya* spp. lipid content differed significantly between ice sections (0-2 vs. 2-5 cm; Table 1) but did not differ between sites (Fig. 3.8B).

Spatially, *Nitzschia frigida* cellular protein content in the 0-2 ice section decreased significantly from sites 1 to 4 (Fig. 3.8C). Vertically, averaged protein content of this species did not significantly differ between ice sections (Table 3.1). *Attheya* spp. (Fig. 3.8D) cellular protein content also decreased significantly from site 1 towards site 4 in the 0-2 cm ice section. Similarly, *Attheya* spp. did not exhibit any significant differences between ice sections for the protein content (Table 3.1).

The lipid:protein ratio for *N. frigida* ratio increased significantly from site 1 to site 4 (Fig. 3.8E). However, no difference in ratio values was observed between ice sections across the sites (Table 3.1). *Attheya* spp. lipid:protein (Fig. 3.8F) also increased significantly from site 1 to site 4. However, in contrast to *N. frigida*, *Attheya* spp. ratio values were found to be significantly different between most ice sections (Table 3.1).

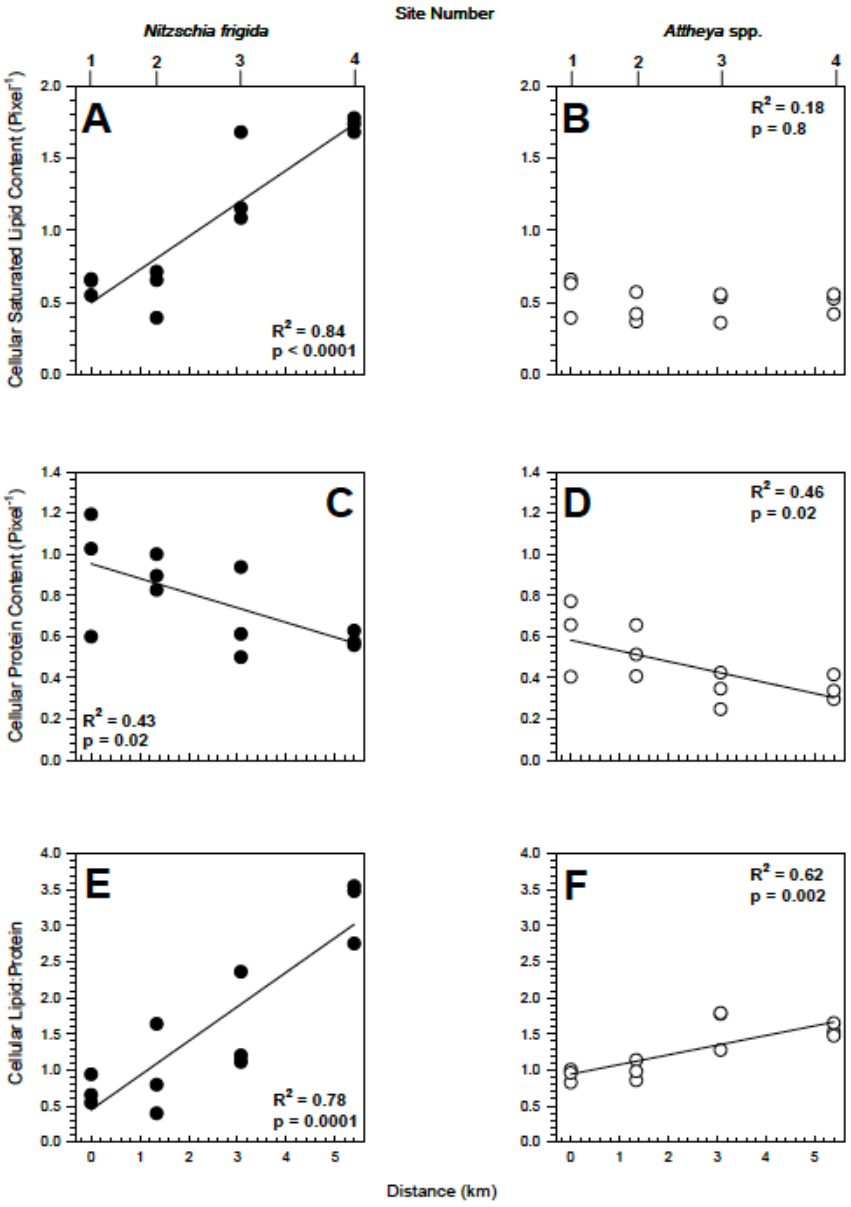


**Figure 3. 8:** *N. frigida* (A, C, and E) and *Attheya* spp. (B, D, and F) biomolecular composition (pixel$^{-1}$) at 0-2 cm per site (1, 2, 3, and 4); A-B) saturated lipid ($y = 0.50 + 0.23x$), C-D) protein ($y = 0.95 - 0.07x$ and $y = 0.58 - 0.05x$), and E-F) saturated lipid:protein ratio ($y = 0.45 + 0.48x$ and $y = 0.94 + 0.13x$). Solid line represents significant linear trend.

**Table 3. 1:** Bulk measurements (i.e. POC, Chla, and POC:Chl *a* ratio) and *Nitzschia frigida* and *Attheya* spp. cellular biomass content (i.e. lipid, protein and lipid:protein ratio) 0-2 cm spatial linear regression (n=12) and 0-2, 2-5, and 5-10 cm vertical two factor repeated measures (i.e. distance, ice section, sample date) analysis across sample sites (n = 35).

| Parameter | POC (mg $m^2$) | Chl *a* (mg $m^2$) | POC:Chl *a* | Cell Count | | Lipid ($pixel^{-1}$) | | Protein ($pixel^{-1}$) | | Lipid:Protein | |
|---|---|---|---|---|---|---|---|---|---|---|---|
| **Ice section (cm)** | | | | *N. frigida* | *Attheya* | *N. frigida* | *Attheya* | *N. frigida* | *Attheya* | *N. frigida* | *Attheya* |
| **0-2** | | | | | | | | | | | |
| Avg. ± SD | 500 ± 170 | 7 ± 3 | 80 ± 20 | $6.4x10^{+07}$ ± $3.6x10^{+07}$ | $5.6x10^{+07}$ ± $1.7x10^{+07}$ | 1.1 ± 0.5 | 0.5 ± 0.1 | 0.8 ± 0.2 | 0.5 ± 0.2 | 1.6 ± 1.1 | 1.3 ± 0.4 |
| **2-5** | | | | | | | | | | | |
| Avg. ± SD | 100 ± 20 | 0.4 ± 0.2 | 290± 80 | $6.2x10^{+05}$ ± $5.5x10^{+05}$ | $8.3x10^{+06}$± $2.6x10^{+06}$ | 1.3 ± 0.4 | 0.8 ± 0.2 | 0.8 ± 0.2 | 0.4 ± 0.1 | 1.9 ± 0.7 | 2.4 ± 0.7 |
| **5-10** | | | | | | | | | | | |
| Avg. ± SD | 70 ± 10 | 0.1 ± 0.04 | 590 ± 130 | $6.7x10^{+04}$± $5.1x10^{+04}$ | $1.8x10^{+06}$± $5.4x10^{+05}$ | 2 ± 2 | 0.7 ± 0.2 | 0.8 ± 0.4 | 0.4 ± 0.1 | 2 ± 3 | 2.0 ± 0.8 |
| **Two Way Repeated Measures ANOVA** | | | | | | | | | | | |
| **Distance** | | | | | | | | | | | |
| **Ice Section** | | | | | | | | | | | |
| F | 85.973 | 37.151 | 67.231 | 8.00‡ | 8.00‡ | 0.522 | 5.245 | 0.0814 | 1.937 | 0.469 | 22.477 |
| p-value | **< 0.001*** | **< 0.001*** | **< 0.001*** | **0.005*** | **<0.001*** | 0.6 | **0.05*** | 0.9 | 0.2 | 0.6 | **0.002*** |
| **Ice Section x Distance** | | | | | | | | | | | |
| **Date** | | | | | | | | | | | |
| F | 6.101 | 0.564 | 3.229 | - | - | 0.297 | 1.001 | 0.303 | 2.454 | 0.562 | 1.535 |
| p-value | **0.04*** | 0.6 | 0.1 | - | - | 0.8 | 0.4 | 0.7 | 0.2 | 0.6 | 0.3 |
| **Date x Distance** | | | | | | | | | | | |
| **Ice Section x Date** | | | | | | | | | | | |
| F | 3.667 | 0.430 | 1.230 | - | - | 0.244 | 1.061 | 0.841 | 0.515 | 0.691 | 0.902 |
| p-value | **0.04*** | 0.8 | 0.3 | - | - | 0.9 | 0.4 | 0.5 | 0.7 | 0.6 | 0.5 |
| **Tukey's Post Hoc Test** | | | | | | | | | | | |
| **0-2 vs 2-5** | | | | | | | | | | | |
| q | 8.552, 7.992, 13.597† | 10.330 | 6.531 | 2.774 | 2.219 | - | 4.569 | - | - | - | 9.355 |
| p-value | **<0.001*** | **0.001*** | **0.009*** | >0.05 | >0.05 | - | **0.04*** | - | - | - | **0.002*** |
| **0-2 vs 5-10** | | | | | | | | | | | |
| q | 9.246, 8.753, 14.334† | 10.771 | 16.292 | 3.883 | 4.438 | - | 2.570 | - | - | - | 6.016 |
| p-value | **<0.001*** | **<0.001*** | **<0.001*** | **<0.05*** | **<0.05*** | - | 0.2 | - | - | - | **0.01*** |
| **2-5 vs 5-10** | | | | | | | | | | | |
| q | 0.694, 0.761, 0.738† | 0.441 | 9.762 | 1.109 | 2.219 | - | 1.999 | - | - | - | 3.339 |
| p-value | >0.8 | 0.9 | **0.001*** | >0.05 | >0.05 | - | 0.4 | - | - | - | 0.1 |

† Difference between ice section within date (i.e. 28 April, 3 May, and 9 May)

‡ Indicates Kruskal-Wallis one-way ANOVA on ranks (0-2, 2-5, and 5-10 cm; n=12)

***** Indicates statistical significance

Note: Difference between date within ice section were observed for 0-2 cm ice section (not shown here)

# 3.5 DISCUSSION

Studies of the ice algal community along a vertical fine structure gradient (Smith et al. 1990, Gradinger 1999), across a tidal strait (Dalman et al. 2019), and over fortnightly tidal cycles (Gosselin et al. 1985, Cota et al., 1987), have helped demonstrate that nutrient supply gradients, via ocean-ice fluxes to the bottom ice algal community, can greatly influence standing stocks and production. However, all of these studies depended on bulk community analyses. The use of FTIR to analyse minute changes in biomolecular composition of bulk algal cells in natural (Giordano et al. 2001, Stehfast et al. 2005, Dean et al. 2010) and culture-based communities (Heraud et al. 2008, Sackett et al. 2013, 2016), as well as individually (Findley et al. 2015; Pogorzelec et al. 2017) have been successful. Here, we examine the biomolecular composition of individual diatom cells, using FTIR spectrochemical imaging, in response to two expected nutrient supply gradients in their natural environment.

### 3.5.1 Bottom-ice algal response across the tidal strait

Light availability to the bottom ice-algal community is greatly attenuated by the high scattering properties and thickness of the overlying snow and sea ice cover, (Perovich et al. 1998, Perovich 2018). Despite our best efforts to target a similar snow depth at all sites, snow depth at site 4 was significantly less in comparison to all other sample sites (Fig. 3.3). However, percent PAR transmittance to the ice bottom was not significantly different, due to a small snow depth difference (<2 cm), an equal surface albedo and increase in ice thickness towards site 4 (~170 cm). The lack of a significant difference in PAR transmittance supported a minimal influence of light variability on algal properties across sites. The lower ice thickness at sites 1 and 2 agreed with the observations of Dalman et al. (2019) where greater under ice tidal currents increased

ocean-ice heat fluxes, impeding ice growth within the tidal strait. In fact, it is this process that has led these regions to be referred to as invisible polynyas (Melling et al. 2015). Support of a greater ocean-ice heat flux also implies a greater nutrient flux from the underlying water column (Dalman et al. 2019), suggesting that we sampled a spatially decreasing nutrient supply gradient from sites 1 to 4. Under-ice currents were not measured during our study.

Dease Strait, including the Finlayson Islands through which the tidal strait was sampled, has been reported to be a nitrogen-deplete environment, limiting local ice algal production (Campbell et al. 2016, Kim et al. *In Review*). The previously determined growth-limiting nutrient, nitrate+nitrite, was consistently <2 μmol $L^{-1}$ and at a mol:mol ratio of 0.27 against silicic acid, indicating nitrogen depletion in the region. This statement is made relative to the adjacent source Pacific water mass, which tends to have a nitrate:silicic acid molar ratio of 0.5, with nitrate concentrations of up to 15 μmol $L^{-1}$ (Carmack et al. 2004). In-ice nutrient concentrations were observed to be greatest in the 0-2 cm ice section (Fig. 3.4B-D), however, no significant difference was observed spatially between sites. There was also no discernable change in pennate diatom contribution to the bottom-ice community composition across the tidal strait (Fig. 3.5). This was in contrast to results from Dalman et al. (2019) who observed a slight decrease in pennate relative abundance away from the tidal strait and hypothesized that the change was a function of decreased ocean-ice nutrient supply (Dalman et al. 2019). Furthermore, only Chl *a* concentration exhibited a significant decrease away from the tidal strait, with no significant trends observed in POC concentration and the POC:Chl *a* g:g ratio (Fig. 3.6). Again, these results make it difficult to conclude a spatial relationship existed across the tidal strait as was observed in Dalman et al. (2019). It is noted that these bulk measurements do not provide information regarding specifics of the ice algal community (such as relative condition of algal

cells) as they include all sea ice inhabitants and organic particulates. In the present study, FTIR spectroscopy analysis was utilized to investigate spatial trends across the tidal strait at the cellular level.

In contrast to the bulk measurements, clear spatial trends were observed in the biomolecular composition of *N. frigida* and *Attheya* spp. cells across the tidal strait. A significant increase in saturated lipid content towards the outside of the tidal strait was observed for *N. frigida*, but no trend was observed across sites for *Attheya* spp. (Fig. 3.8A and B). In contrast, cellular protein content and the lipid:protein ratio significantly decreased and increased, respectively, outside of the tidal strait for both *N. frigida* and *Attheya* spp. (Fig. 3.8 C-F).

Photosynthate allocation of carbon within the cell can be altered by either light availability and or nutrient stress (Smith et al. 1997, Mock & Kroon 2002a, b). During the early portion of the bloom, when the nutrient supply is higher relative to the algal standing stock, and thus nutrient demand (Gradinger 2009, Dalman et al. 2019), ice algae divert photosynthesis-assimilated carbon to protein production. When nutrients become limiting, the allocation of carbon is diverted away from protein production and protein enriched complexes, such as the chloroplast's photosystem II, to lipid production (Smith et al. 1997, Giordano et al. 2001, Mock & Kroon 2002a, Stehfest et al. 2005). The latter response is also expected to increase with increasing light availability (Mock & Kroon 2002b). The fact that no significant difference in PAR transmittance was observed across sites in our study decreases the likelihood of mis-identifying biomolecular changes as a result of light availability. The observed changes in biomolecular composition of both *N. frigida* and *Attheya* spp. cells could thus be interpreted as a response to nutrient deficiency within the ice algal community. Therefore, these results support the existence of a greater nutrient supply towards the centre of the tidal strait as concluded in

Dalman et al. (2019). Furthermore, the greater response of lipid content in *N. frigida* cells relative to that of *Attheya* spp. cells across the tidal strait supports greater sensitivity to changes in nutrient availability as a function of the larger size and greater nutrient demand of *N. frigida* cells (Pogorzelec et al. 2017).

### 3.5.2 Ice algal response up into the bottom-ice matrix

Nutrient, POC and Chl *a* concentrations all significantly decreased away from the ocean-ice interface (from 0-2 to 5-10 cm). Within the bottom-ice 2-10 cm section, algae were starved of nutrients, with averaged nitrate+nitrite, silicic acid, and phosphate concentrations of 0.3, 1.3, and 0.2 μmol $L^{-1}$, respectively. The difference vertically between ice sections was accentuated when comparing the POC:Chl *a* g:g ratio, which increased from <100 in the bottom 0-2 cm section to >450 in the 5-10 cm section. Lower values of the POC:Chl *a* ratio can be used to indicate a greater contribution of active photosynthetic cells to the POC pool, with the ratio slightly increasing under greater light availability due to decreased pigment production with light acclimation and greater lipid production (Gosselin et al. 1990, Kirst and Wiencke 1995, Mock and Kroon 2002b). However, substantial increases should be associated with nutrient stress and a change from autotrophic to heterotrophic community state, such as arises during post-bloom conditions (Mock and Kroon 2002a). The significant increase in the POC:Chl *a* ratio away from the ocean-ice interface likely indicated a mostly trapped ice algal community that was in a post bloom state with depleted nutrient resources.

Higher into the bottom-ice matrix, centric diatoms increased in relative abundance to become the dominant taxa, even though a significant decrease in absolute abundance was observed for all algal cells. Other ice algal taxa (e.g. flagellates and dinoflagellates) also increased in relative

contribution as was observed in Gradinger (1999). Dominance by the smaller centric diatom cells has been explained by less stress under nutrient-limiting conditions relative to that of larger pennate cells, such as *N. frigida* (Pogorzelec et al. 2017, Campbell et al. 2018), or by an increase in light availability (Różańska et al. 2009). With respect to light availability, assuming an ice attenuation coefficient of ~2 $m^{-1}$ (Perovich et al. 1998), the difference between the ice bottom and 10 cm up into the ice matrix would be ~0.5% of surface irradiance. This difference fits within the range of PAR transmittance observed across our sites. However, a slightly greater attenuation coefficient is likely more reasonable to take into account the bulk ice algal concentration over the bottom 0-10 cm, which equates to 70 mg $m^{-3}$ (Table 3.1). Using the equation provided in Ehn and Mundy (2013), an attenuation coefficient of 5.4 $m^{-1}$ is obtained for this Chl *a* concentration, which equates to a change of ~1.5% of surface irradiance over the 10-cm ice-bottom section. This vertical change in light availability is slightly greater than the spatial variability, and thus cannot be ignored in its potential influence on the algal community. However, it is significant to note that the vertical change in nutrient concentration was much greater than its spatial variability, supporting a greater influence of decreasing nutrient availability up into the ice bottom (Fig. 3.4B-D, Table 3.1).

Indeed, the increase in proportion of empty pennate frustules, but not centric frustules, suggests a greater stress on the larger pennate cells. However, the biomolecular response suggests a different possibility. *N. frigida* only increased in lipid content vertically from the 0-2 to 2-5 cm section (Table 3.1). In contrast, *Attheya* spp. lipid content significantly increased from the 0-2 cm section to both the 2-5 and 5-10 cm sections. Additionally, only *Attheya* spp. lipid:protein ratio significantly increased across all ice sections. These results suggest a greater stress on *Attheya* spp. cells higher up into the ice matrix. As discussed above, when nutrients

(particularly nitrogen) become limiting, protein production is reduced and a greater allocation of carbon to lipid production occurs (Smith et al. 1997, Mock & Kroon 2002a, Pogorzelec et al. 2017). It is hypothesized that the *Attheya* spp. cells were trapped and cut-off from any nutrient supply; a change in protein content would not be expected as cells would not be growing and dividing. However, continued photosynthesis by individual cells could result in increased lipid production as observed in our results. The vertical change in *Attheya* spp. biomolecular composition and the lesser response of that by *N. frigida* cells are somewhat counterintuitive relative to the taxonomic composition observations that suggested a shift towards centric diatom community dominance away from the ocean-ice interface. The discrepancy between the relative increase in *N. frigida* empty frustules versus no change for that in *Attheya* spp. can potentially be explained by sample processing. That is, the thin and fragile *Attheya* spp. frustules could have been more easily broken-down during sample processing and storage and thus indiscernible during cell enumeration. It is also noted that epiphytic associations between *Attheya* spp. and much larger pennate cells (Poulin et al. 2011) were only observed in the 0-2 cm ice section. It has been suggested that the host diatom can provide a transfer of nutrients to the epiphytic diatom (Cattaneo & Kalff 1979, Eminson & Moss 1980). Therefore, we surmise that a lack of epiphytic host higher into the ice, combined with a very limited ambient nutrient access, could have greatly influenced the individual *Attheya* spp. cells metabolic functions (i.e. lipid:protein ratio).

The lack of vertical change in *N. frigida* lipid:protein content could also be due to a multiple factors. Firstly, *N. frigida* can decrease metabolism (Aletsee and Jahnke 1992, Zhang et al. 1995) and potentially exhibit a heterotrophic strategy, utilizing previously extruded extracellular polymeric substance (EPS) as a nutrient resource (Nemi et al. 2011). These strategies could

minimize changes in biomolecular composition vertically in the ice matrix. Secondly, as a raphid pennate diatom (Medlin and Hasle 1990), *N. frigida* has the capacity to glide across surfaces (Wetherbee et al. 1998). Indeed, the capacity of sea ice pennate diatoms to move vertically through the sea ice matrix in response to changes in light and nutrient access has been demonstrated (Aumack et al. 2014). The potential for vertical motility of *N. frigida* cells could mask any vertical response of this taxa within the bottom ice matrix and the opposite for non-motile centric diatoms (e.g., *Attheya* spp.) that would be trapped in place within the accreting bottom-ice environment.

Additional work is required to fully elucidate the physical and biological processes that led to our observations. However, it is important to note that without the FTIR technique and its corresponding cellular biomass composition estimates, interpretation of the vertical response of the ice algal community would have been substantially limited. This note also applies to the spatial results where changes in biomass composition strongly supported the existence of a nutrient gradient across the Finlayson Islands tidal strait, whereas the bulk measurements (i.e., POC, Chl *a* and POC:Chl *a* ratio) made it difficult to draw conclusions from. Application of FTIR spectroscopy for the autecological research of diatoms is still a relatively new and rarely used technique. Therefore, we strongly encourage application of the technique to future ecological studies of sea ice diatoms.

## 3.6 ACKNOWLEDGEMENTS

This study was supported by funding from the Northern Scientific Training Program award to N.M.P., Natural Science and Engineering Research Council of Canada (NSERC) Discovery Grants to C.J.M. and K.M.G. and Northern Research Supplement to C.J.M, and the Kitikmeot

Region Marine Science Study, a Polar Knowledge Canada grant to the Arctic Research Foundation (ARF). Field and laboratory instruments from the Arctic Biogeochemical Optics Laboratory (ABOL) were originally purchased through Canada Foundation for Innovation grants. FTIR was purchased with assistance from and Western Economic Diversification Canada (Winnipeg Partnership Agreement) and the University of Manitoba Faculties of Science and Engineering. Special thanks are extended to David Capelle for MATLAB support, Canada High Arctic Research Station (CHARS) operated by Polar Knowledge Canada for logistic support and housing, the Ekaluktutiak Hunters and Trappers Organization, and the community of Cambridge Bay, Nunavut, CA for supporting the research conducted during the 2017 ICE-CAMPS field campaign. ICE-CAMPS is a contribution to the Arctic Science Partnership (ASP).

# 3.7 REFERENCES

Aletsee, L., and Jahnke, J., (1992) Growth and productivity of the psychrophilic marine diatoms Thalassiosira antarctica Comber and Nitzschia frigida Grunow in batch cultures at temperatures below the freezing point of sea water. Polar biology, 11(8): 643-647

Aumack, C.F., Juhl, A.R., Krembs, C., (2014) Diatom vertical migration within land-fast Arctic sea ice. Journal of Marine Systems, 139: 496-504

Arrigo, K.R., (2014) Sea ice ecosystems. Annu. Rev. Mar. Sci., 6:439-67. doi: 10.1146/annurev-marine-010213-135103

Campbell, K., Mundy, C.J., Landry, J.C., Delaforge, A., Michel. C., Rysgaard, S., (2016) Community dynamics of bottom-ice algae in Dease Strait of the Canadian Arctic. Prog. Oceanogr., 149:27-39

Campbell, K., Mundy, C. J., Belzile, C., Delaforge, A., Rysgaard, S., (2018) Seasonal dynamics of algal and bacterial communities in Arctic sea ice under variable snow cover. Polar Biology, 41(1), 41-58

Cattaneo, A., and Kalff,I., (1979) Primary production of algae growing on natural and arti- ficial aquatic plants. A study of interactions between epiphytes and their substrate. LimnoL Oceanogr., 24: 1031-1037

Carmack, E.C., Macdonald, R.W. and Jasper, S., (2004) Phytoplankton productivity on the Canadian Shelf of the Beaufort Sea. Marine Ecology Progress Series, 277, pp.37-50

Comiso, J.C., Parkinson, C.L., Gersten, R. and Stock, L., (2008) Accelerated decline in the Arctic sea ice cover. Geophys. Res. Lett., 35: L01703. doi: 10.1029/2007GL031972

Cota, G.F., Prinsenberg, S.J., Bennett, E.B., Loder, J.W., Lewis, M.R., Anning, J.L., Watson, N.H.F., Harris, L.R., (1987) Nutrient fluxes during extended blooms of Arctic ice algae. J Geophys Res-Oceans 92(C2): 1951-1962.

Cutter, C., Andersson, P., Codispoti, L., Croot, P., Francois, R., Lohan, M.C., Obata, H. and Rutgers van der Loeff, M., (2014) Sampling and sample-handling protocols for GEOTRACES cruises, v. 2.0., GEOTRACES, pp 123-125

Dalman, L.A., Else, B.E., Barber, D., Carmack, E., Williams, W.J., Campbell, K., Duke, P.J., Mundy, C.J., (2019) Enhanced ice algal biomass along a tidal strait gradient in the lower Northwest Passage of the Canadian Arctic. Elementa: Science of the Anthropocene (in review).

Dean, A.P., Sigee, D.C., Estrada, B., Pittman, J.K., (2010) Using FTIR spectroscopy for rapid determination of lipid accumulation in response to nitrogen limitation in freshwater microalgae. Bioresource Technol 101: 4499−4507

Eminson, D., and Moss, B., (1980) The composition and ecology of periphyton communities in freshwaters: 1 the influence of host type and external environment on community composition. *British Phycological Journal*, *15*(4): 429-446

Ehn, J.K. and Mundy, C.J., (2013) Assessment of light absorption within highly scattering bottom sea ice from under-ice light measurements: Implications for Arctic ice algae primary production. Limnology and Oceanography, 58(3): 893-902

Findlay, C.R., Wiens, R., Rak, M., Sedlmair, J., Hirschmugl, C.J., and others (2015) Rapid biodiagnostic ex-vivo imaging at 1 μm pixel resolution with thermal source FTIR FPA. Analyst 140:2493 – 2503

Garrison, D.L., and Buck, K.R., (1986) Organism losses during ice melting: a serious bias in sea ice communities studies. Polar Biol 6:237-239

Giordano, M., Kansiz, M., Heraud, P., Beardall, J., Wood, B., and McNaught, D., (2001) Fourier transform infrared spectroscopy as a novel tool to investigate changes in intracellular macromolecular pools in the marine microalga Chaetoceros Muellerii (Bacillariophyceae). J. Phycol. 37:271-279

Gosselin, M., Legendre, L., Demers, S. and Ingram, R.G., (1985) Responses of sea-ice microalgae to climatic and fortnightly tidal energy inputs (Manitounuk Sound, Hudson Bay). Canadian Journal of Fisheries and Aquatic Sciences, 42(5): 999-1006

Gosselin, M., Legendre, L., Therriault, J.C., Demers, S., (1990) Light and nutrient limitation of sea-ice microalgae (Hundson Bay, Canadian Arctic). J Phycol 26: 220−232

Gradinger, R., (1999) Vertical fine structure of the biomass and composition of algal communities in Arctic pack ice. Marine Biology 133:745-754

Gradinger, R., (2009) Sea-ice algae: Major contributors to primary production and algal biomass in the Chukchi and Beaufort Seas during May/June 2002. Deep Dea Res 11 56(17): 1201–1212.

Grasshoff, K, Kremling, K, Ehrhardt, M., (1999) Methods of seawater analysis. 3rd ed. New York, NY: Wiley-VCH.

Griffiths, P., and de Haseth, J., (2007) Fourier Transform Infrared Spectrometry, 2nd edn. Wiley Inter-Science, New Jersey

Heraud, P., Stojkovic, S., Beardall, J., McNaughton, D., Wood, BR., (2008) Intercolonial variability in macromolecular composition in P-starved and P-replete Scenedesmus populations revealed by infrared microspectroscopy. J Phycol 44: 1335−1339

Holm-Hansen, O., Lorenzen, C.J., Holmes, R.W., Strickland, J.D.H., (1965) Fluorometric Determination of Chlorophyll. ICES Journal of Marine Science 30(1), 3-15

Horner, R., Ackley, S.F., Dieckmann, G.S., Gulliksen, B., Hoshiai, T., Legendre, L., Melnikov, I.A., Reeburgh, W.S., Spindler, M. and Sullivan, C.W., (1992) Ecology of sea ice biota: 1. Habitat, terminology, and methodology. Polar Biol, 12:417-427

Kirst, G.O., and Wiencke, C., (1995) Ecophysiology of polar algae. J Phycol 31: 181−199

Leu, E., Wiktor, J., Søreide, J.E., Berge, J., Falk-Petersen, S., (2010) Increased irradiance reduces food quality of sea ice algae. MAR ECOL-PROG SER 411:49-60

Leu, E., Mundy, C.J., Assmy, P., Campbell, K., Gabrielsen, T.M., Gosselin, M., Juul-Pedersen, T. and Gradinger, R., (2015) Arctic spring awakening-steering principles behind the phenology of vernal ice algae blooms. Progress in Oceanography, 139:151-170

Lund, J.W.G., Kipling, C., and E.D. Le Cren (1958), The inverted microscope method of estimating algal number and the statistical basis of estimations by counting, Hydrobiol. 11, 143–170, doi:10.1007/BF00007865.

Markus, T., Strieve, J.C., and Miller, J., (2009) Recent changes in Arctic sea ice melt onset, freezeup, and melt season length. Journal of Geophysical research, 114:C12024

Medlin, L.K. and Hasle, G.R., (1990) Some Nitzschia and related diatom species from fast ice samples in the Arctic and Antarctic. Polar Biology, 10(6):451-479

Melling, H., Haas, C. and Brossier, E., (2015) Invisible polynyas: Modulation of fast ice thickness by ocean heat flux on the Canadian polar shelf. Journal of Geophysical Research: Oceans, 120(2): 777-795

Michel, C., Ingram, R.G., Harris, L.R., (2006) Variability in oceanographic and ecological processes in the Canadian Arctic Archipelago. Progress in Oceanography, 71:379-401

Mock T, Gradinger R (2000) Changes in photosynthetic carbon allocation in algal assemblages of Arctic sea ice with decreasing nutrient concentration and irradiance. MAR ECOL-PROG SER 202:1-11

Mock, T., Kroon B.M.A., (2002a) Photosynthetic energy conversion under extreme conditions-I: important role of lipids as structural modulators and energy sink under *N*-limited growth in Antarctic sea ice diatoms. Phytochemistry, 61: 41-51

Mock, T., Kroon B.M.A., (2002b) Photosynthetic energy conversion under extreme conditions-II: the significant of lipids under light limited growth in Antarctic sea ice diatoms. Phytochemistry, 61: 53-60

Mock, T., Thomas, D.N., (2005) Recent advances in sea-ice microbiology. Environmental Microbiology, 7(5):605-619

Mundy, C.J., Barber, D.G. and Michel, C., (2005) Variability of snow and ice thermal, physical and optical properties pertinent to sea ice algae biomass during spring. Journal of Marine Systems, 58:107-120

Niemi, A., Michel, C., Hille, K. and Poulin, M., (2011) Protist assemblages in winter sea ice: setting the stage for the spring ice algal bloom. Polar Biology 34:1803-1817

NSIOC (2018) Daily image update. Accessed on June 11 2018. Nsidc.org/arcticsciencenews/

Parsons, T.R., Maita, Y., and Lalli, C.M., (1984), Manual of chemical and biological methods for seawater analysis. Pergamon Press, New York

Pogorzelec, N.M., Mundy, C.J., Findlay, C.R., Campbell, K., Diaz, A., Ehn, J.K., Rysgaard, S. and Gough, K.M., (2017) FTIR imaging analysis of cell content in sea-ice diatom taxa during a spring bloom in the lower Northwest Passage of the Canadian Arctic**.** MEPS, 69:77-88

Perovich, D.K., Roesler, C.S., Pegau, W.S., (1998) Variability in Arctic sea ice optical properties. J Geophys Res Oceans 103: 1193−1208

Perovich, D.K., (2018) Sunlight, clouds, sea ice, albedo, and the radiative budget: the umbrella versus the blanket. *The Cryosphere*, *12*(6), pp.2159-2165.

Poulin, M., Daugbjerg, N., Gradinger, R., Ilyash, L., Ratkova, T., and others (2011) The pan-Arctic biodiversity of marine pelagic and sea-ice unicellular eukaryotes: a first-attempt assessment. Marine Biodiversity 41:(1)13-28

Rintala, J.M., Piiparinen, J., Blomster, J., Majaneva, M., Müller, S., Uusikivi, J. and Autio, R., (2014) Fast direct melting of brackish sea-ice samples results in biologically more accurate results than slow buffered melting. Polar Bio, DOI 10.1007/s00300-014-1563-1

Różańska M., Gosselin M., Poulin M., Wiktor J.M., Michel, C., (2009) Influence of environmental factors on the development of bloom ice protest communities during the winter-spring transition. MAR ECOL-PROG SER 386:43-59

Sackett, O., Petrou, K., Reedy, B., De Grazia, A., and others (2013) Phenotypic plasticity of Southern Ocean diatoms: key to success in the sea ice habitat? PLOS ONE 8: e81/85

Sackett, O., Petrou, K., Reedy, B., Hill, R., and others (2016) Snapshot prediction of carbon productivity, carbon and protein content in Southern Ocean diatom using FTIR spectroscopy. ISME J 10: 416−426

Sattar, A. and Alexander, J.C., (1976) Effect of wavelength on light induced quality of deterioration of edible oils and fats. Can. Inst. Food Sci. Technol. J. 9:180-113

Smith, R.E.H., Clement, P., Cota, G.F., Li, W.K., (1987) Intercellular photosynthate allocation and the control of Arctic marine ice algal production. J PHYCOL 23:124-132

Smith, R.E.H., Harrison, W.G., Harris, L.R., and Herman, A.W., (1990) Vertical fine structure of particulate matter and nutrients in sea ice of the high Arctic. Can J. Fish. Aquat. Sci. 47:1348-1355

Søreide, J.E., Leu, E.V.A., Berge, J., Graeve, M., and Falk-Petersen, S.T.I.G., (2010) Timing of blooms, algal food quality and Calanus glacialis reproduction and growth in a changing Arctic. Global Change Biology 16:3154-3163

Stehfest. K., Toepel, J., Wilhelm, C., (2005) The application of micro-FTIR spectroscopy to analyse nutrient stress related changes in biomass composition of phytoplankton algae. Plant Physiol Bioch 43: 717−726

Stitt, D.M., Kastyak-Ibrahim, M.Z., Liao, C.R., Morrison, J., Albensi, B.C., Gough, K.M., (2012) Tissue acquisition and storage associated oxidation considerations for FTIR microspectroscopic imaging of polyunsaturated fatty acids. Vibrational Spectroscopy 60:16-22

Stroeve, J.C., Serreze, M.C., Holland, M.M., Kay, J.E., Malanik, J., and Barrett, A.P., (2012) The Arctic's rapidly shrinking sea ice cover: a research synthesis. Climate Change 110:1005-1027, doi 10.1007/s10584-011-0101-1

Tedesco, L., Vichi, M., and Scoccimarro, E., (2019) Sea-ice algal phenology in a warmer Arctic. Science Advances 5(5):4830

Vancoppenolle, M., Meiners, K.M., Michel, C., Bopp, L., Brabant, F., Carnat, G., Belille, B., Lannuzel, D., Madec, G., Moreau, S., Tison, J.L., van der Merwe, P. (2013) Role of sea ice in global biogeochemical cycles: emerging views and challenges. Quaternary Sci Rev 79, 207-230.

Van Leeuwe, M.A., Tedesco, L., Arrigo, K.R., Assmy, P., Campbell, K., Meiners, K.M., Rintala, J-M., Selz, V., Thomas, D.N., Stefels, J. (2018) Microalgal community structure and primary production in Arctic and Antarctic sea ice: A synthesis. Elem Sci Anth 6:4. doi: https://doi.org/10.1525/elementa.267

Wetherbee, R., Lind, J.L., Burke, J., and Quatran, R.S., (2007) Sea-ice algae in Arctic pack ice during late winter. Polar Bio., 30:1493-1504

Zhang, Q., Gradinger, R., Spindler, M., (1998) Dark survival of marine microalgae in the high Arctic (Greenland Sea). Polarforsch 65:111–116

# 3.8 SUPPLEMENTAL MATERIAL

**Supplemental Table 3. 1**: Salinity and inorganic nutrients spatial and vertical paired t-test analysis across sample sites.

| Parameter<br>Ice section (cm) | Salinity (psu)<br>n = 12 | Phosphate (µmol $L^{-1}$)<br>n = 12 | Nitrate + Nitrite (µmol $L^{-1}$)<br>n = 12 | Silicic Acid (µmol $L^{-1}$)<br>n = 12 |
|---|---|---|---|---|
| **0-2** | | | | |
| Avg. ± SD | 9.9 ± 1.6 | 4.9 ± 2.0 | 1.5 ± 0.9 | 5.4 ± 2.3 |
| **2-5** | | | | |
| Avg. ± SD | 6.5 ± 0.6 | 0.3 ± 0.06 | 0.3 ± 0.2 | 1.7 ± 0.7 |
| **5-10** | | | | |
| Avg. ± SD | 6.0 ± 0.4 | 0.2 ± 0.06 | 0.4 ± 0.2 | 0.9 ± 0.5 |
| **Two Way Repeated Measures ANOVA** | | | | |
| **Distance** | | | | |
| **Ice Section** | | | | |
| F | 472.469 | 72.798 | 104.808 | 22.257 |
| p-value | **< 0.001*** | **< 0.001*** | **< 0.001*** | **0.002*** |
| **Ice Section x Distance** | | | | |
| **Date** | | | | |
| F | 5.920 | 0.798 | 3.770 | 0.204 |
| p-value | **0.04*** | 0.5 | 0.9 | 0.8 |
| **Date x Distance** | | | | |
| **Ice Section x Date** | | | | |
| F | 5.572 | 0.764 | 1.964 | 0.287 |
| p-value | **0.009*** | 0.569 | 0.164 | 0.881 |
| **Tukey's Post Hoc Test Ice Section within Date** | | | | |
| **0-2 vs 2-5** | | | | |
| q | 16.189, 7.246, 12.857† | 14.620 | 18.694 | 7.217 |
| p-value | **<0.001*** | **<0.001*** | **<0.001*** | **0.005*** |
| **0-2 vs 5-10** | | | | |
| q | 18.405, 8.785, 14.661† | 14.932 | 16.580 | 4.573 |
| p-value | **<0.001*** | **<0.001*** | **<0.001*** | **0.002*** |
| **2-5 vs 5-10** | | | | |
| q | 2.216, 1.540, 1.803† | 0.312 | 2.114 | 1.655 |
| p-value | >0.05 | 1.0 | 0.4 | 0.511 |
| **Tukey's Post Hoc Test Date within Ice Section** | | | | |
| **28 April vs. 3 May** | | | | |
| q | 7.854, 1.997, 1.690‡ | - | - | - |
| p-value | **<0.001***, 0.359, 0.473 | - | - | - |
| **28 April vs. 9 May** | | | | |
| q | 4.473, 1.206, 0.703‡ | - | - | - |
| p-value | >0.05 | - | - | - |
| **3 May vs. 9 May** | | | | |
| q | 3.381, 0.791, 0.987‡ | - | - | - |
| p-value | >0.05 | - | - | - |

† Ice section within date (0-2, 2-5, and 5-10 cm)
‡ Date within ice section (28 April, 3 May, and 9 May)
***** indicates statistical significance

# CHAPTER 4: FTIR ANALYSIS OF THE BULK DIATOM COMMUNITY

## 4.1 INTRODUCTION

Diatoms (*Bacillariophyceae*) are the dominant taxa of Arctic ice algae (Poulin et al. 2011) and of most phytoplankton blooms during the polar spring (Leu et al. 2015). These pulses of primary production support an energy-demanding Arctic marine ecosystem (Michel et al. 2006, Søreide et al. 2010, Arrigo 2014) in which diatoms produce high-energy essential fatty acids (i.e. saturated and unsaturated fats; Mock & Thomas 2005, Leu et al. 2010, Søreide et al. 2010). Diatoms are a unique unicellular species of algae whose "shell" is a glass-like matrix composed of biogenic silica called a frustule. The shape and form of their frustule can be used to further classify diatoms into two common sub-categories; pennate (bilateral symmetric) and centric (radial symmetric) diatoms, with pennates being the most dominant form found in sea ice (Round et al. 1990, Poulin et al. 2011), while centric diatoms tend to dominate Arctic phytoplankton blooms (Arrigo et al., 2012, Mundy et al., 2014). A rapidly warming Arctic, causing earlier and longer sea ice melting seasons (Comiso et al. 2008, Markus et al. 2009, Stroeve et al. 2012), is strongly altering the habitat of both ice algae and phytoplankton. This warming results in a shift in timing, magnitude, and fate of each bloom, and will have important ramifications on the Arctic marine ecosystem as a whole.

Fourier Transform Infrared (FTIR) spectrochemical imaging is a non-destructive, sensitive, and efficient analytical infrared (IR) imaging technique that has been used successfully for the analysis of the biomolecular composition of diatom cells (Giordano et al. 2001, Stehfast et al. 2005, Heraud et al. 2008, Dean et al. 2010, Sackett et al. 2013, 2016, Findley et al. 2015, Pogorzelec et al. 2017). It has been well established that the infrared spectra of diatoms exhibit

strong bands associated with saturated lipid ($CH_2$+$CH_3$ stretches : 2980 and 2840 $cm^{-1}$), protein (Amide I: centred ~1645 $cm^{-1}$) and silica (Si-O: 1075 $cm^{-1}$); occasionally polyunsaturated lipid (PUFA: 3008 $cm^{-1}$) is also detected (Pogorzelec et al. 2017). Cellular lipid production is affected by both light and nutrient availability (Gosselin et al. 1990, Mock & Gradinger 2000, Mock & Kroon 2002a, b), whereas cellular protein production has been found to be mainly affected by nutrient availability (Gosselin et al. 1990, Mock & Kroon 2000a). Therefore, the relative intensities of spectral bands for lipid and protein can serve as biomarkers for monitoring the effects of light and nutrient availability on the ice algal community, over time.

The speed at which FTIR image acquisition is accomplished could be greatly improved, especially for the measurements of the bulk ice algal community. Herein, we describe an FTIR analysis technique that enables rapid, efficient, and precise estimates of the biomolecular composition of the diatom community. We have recorded and analysed the biomass composition of a sample population from a diatom community, comparing results from a Focal Plane Array (FPA) and a Single Element (SE) detector, in order to determine the method that would best represent the community's biomolecular composition in an efficient manner. Diatom cells for the study were obtained from a bottom-ice algal community collected during the 2017 Ice Covered Ecosystem-Cambridge Bay Process Study (ICE-CAMPS).

# 4.2 MATERIALS AND METHODS

## 4.2.1 Field Collection

Samples were collected during the 2017 ICE-CAMPS field campaign, between the Finlayson Islands (a tidal strait region; 69°00.033'N, 105°48.967'W) within Dease Strait, and near Cambridge Bay, NU, Canada, over three days between 26 April and 9 May. Ice cores were

collected on landfast sea ice using a 9-cm inner diameter Mark II Coring System (Kovacs Enterprises). Ice algal samples were collected by sectioning the lower 2 and 10 cm of ice cores under thin (<4 cm) snow cover. Sample sites consisted of sites 1, 2, 3 and 4 across a constricted waterway between the Finlayson Islands, herein after referred to as a tidal strait (Dalman et al. 2019; refer to Chapter 3; Fig. 4.1). To minimize the effects of visible and UV radiation on the biomolecular composition of the ice algal samples (Leu et al. 2010, Stitt et al. 2012), all ice cores were shaded during collection and segmentation. Ice cores were collected (1-3 cores) and pooled together for each site and placed into insulated containers for transport and melting. Upon returning to the laboratory, 0.2-µm membrane filtered seawater (FSW) was added to each container to create a 3:1 ratio of FSW to ice cores. The FSW and ice core solution was left to melt naturally in insulated containers (Rintala et al. 2014). The FSW was added in order to minimize fresh water osmotic shock and reduce the probability of algal cell-lysis (Garrison & Buck 1986, Rintala et al. 2014), due to pure ice core melt.

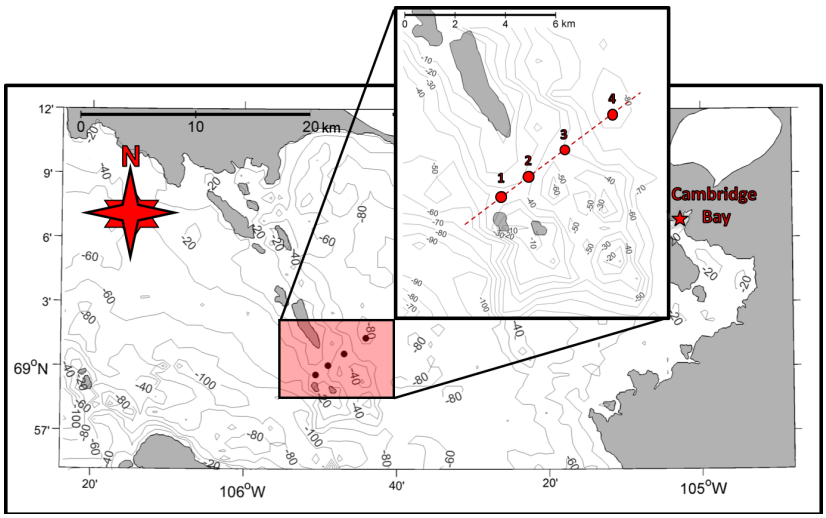


**Figure 4. 1:** 2017 ICE-CAMPS sample site locations (*26 April to 9 May*) in the Dease Strait between the Finlayson Islands, near Cambridge Bay, Nunavut, Canada (*69°00.033'N, 105°48.967'W)*. FTIR SE bulk community measurements included sites 1, 2 and 4 (0-10 cm). FPA bulk 0-2 cm community and 0-10 cm single cell methods were tested with cells from, included sites 1, 2, 3, and 4.

### 4.2.2 Bulk Community FTIR Sample Preparation

FSW-ice core solution, between 15 and 60 ml, was filtered onto a 5-µm pore, 25-mm polycarbonate membrane filter (*SterliTech Corp. USA*) for later FTIR analysis. Filters were folded in half, wrapped in a pre-labelled aluminium casing, and stored at -80°C for up to 18 months prior to analysis. The technique described here closely follows that of the diatom-FTIR procedures that have been described elsewhere in more detail (Findlay et al. 2015, Pogorzelec et al. 2017, *refer to Chapter 3*). All FTIR samples were prepared in a darkened environment to minimize light exposure. Diatoms were released from the polycarbonate filters and onto a 25 mm diameter, 1 mm thick calcium fluoride ($CaF_2$; single element experiment) or 2 mm thick barium fluoride ($BaF_2$; focal plane array experiment) crystal substrate. Several 4 µl Milli-Q water droplets were applied to the surface with a micropipette; a portion of the filter (roughly ¼) was placed against the droplet, agitated, and quickly removed to release the cells. The cells were left suspended in the droplet for roughly 30 seconds in order for them to settle to the substrate. After, the excess water was carefully wicked away with lens tissue (low water absorption). This technique greatly reduced the formation of sea salt crystals, which can negatively impact FTIR spectral quality. The diatoms were examined under a white light microscope, coupled with a red-light-photo-filter (650 nm) over the light source, to assess diatom abundance and location across the window. The red-light-photo-filter was used to prevent or at least reduce, the photo-oxidation of biomolecular content (Sattar et al. 1976, Stitt et al. 2012) within diatom cells. Before FTIR analysis, cells were placed in a dark desiccator and dried for about 18 hrs to remove IR-active water molecules from the sample.

### 4.2.3 FPA Bulk FTIR Spectrochemical Imaging

An Agilent Cary 670 FTIR Spectrometer and a 620 IR Imaging Microscope was used to analyse the diatom community biomolecular composition in transmission mode. This mode refers to the IR light passing through the sample and IR-inactive crystal substrate. Infrared light may be absorbed by the sample when the vibrational energies of the molecular functional groups match the IR electromagnetic wavelengths. The IR light that is not absorbed travels to the detector; the result is first recorded as percent transmittance, then converted into absorbance, via Beer's Law ((Absorbance = -log [%Transmittance]); Griffiths & de Haseth, 2007). All bulk spectra of diatom cells were obtained with a 15x, 0.62 numerical aperture (NA) objective and condenser. The FPA bulk imaging technique required the use of a focal plan array (FPA). An FPA detector projects the entire imaged area onto a 64 x 64-pixel array of detectors, to yield 4096 individual IR spectra. The field of view (FOV) on the sample is 352 x 352 μm, thus each IR spectrum comes from an area of 5.5 x 5.5 μm, at normal magnification. For this study, the entire spectra array was binned to produce a single summed IR spectrum (containing between 30 to 100 cells) of an entire FOV. A sum of 512 background scans or "blank image" was first collected from a clean FOV; bulk diatom spectra were collected as a sum of 256 co-addition scans and ratioed to the background.

### 4.2.4 FPA Single Cell FTIR Spectrochemical Imaging

Similar procedures (as described above) were followed for the FPA single cell technique. Individual diatom cells of *N. frigida* (average cell size of 68 x 8 μm) and *Attheya* spp. (average cell size of 9 x 10 μm) were imaged using the high magnification optics (geometric pixel area: 1.1 x 1.1 μm), with a FOV of 70.4 x 70.4 μm. Depending on the size of the diatom, 1 to 3

diatoms could be imaged within a single FOV. Single celled diatoms were imaged at a sum of 512 background scans and 256 co-addition scans. Final FTIR image spectra were imported into Matlab™ for further processing (Finlay et al. 2015, Pogorzelec et al 2017).

### 4.2.5 Single Element Bulk FTIR Spectrochemical Imaging

Bulk spectra of diatom cells, about 50 to 200 cells per field of view (FOV), were obtained within a Single Element detector (SE). Unlike an FPA detector, a SE detector produces a single IR spectrum from the entire FOV area (~530 x 440 μm; Fig. 4.2). As the SE FOV is larger than the FPA (both in high and normal mag), 50 to 200 cells could be captured at a time within a single SE image. For all SE bulk diatom community data, a background was first collected as a sum of 256 scans from a FOV that had no diatoms present. Bulk diatom community spectra were then collected as a sum of 128 co-addition scans and ratioed to the background to obtain the final FTIR spectrum.

### 4.2.6 Bulk Diatom Community FTIR Spectral Analysis

The saturated lipid, protein, and silica band areas were determined by integration of the area under the absorption band of the spectral peaks to establish the total integrated biomass content of the community, illustrated for SE imaging in Fig. 4.2 (*refer to Chapter 3 for band integrations parameters*). The number of diatom cells in each FOV or per FTIR image/spectrum were counted from a light microscope image. Diatoms were counted to whole numbers (no fractions) by placing a 5 x 4 grid on the photo of the imaged area and manually counting the number of diatoms within each cell of the grid. Damaged cells were counted only if ≥50% of the cell

remained intact. For the single cell FPA technique, spectra were summed on a per cell basis for *Attheya* spp. and *N. frigida*, via Matlab$^{TM}$ processing (Pogorzelec et al. 2017; *refer to Chapter 3*)

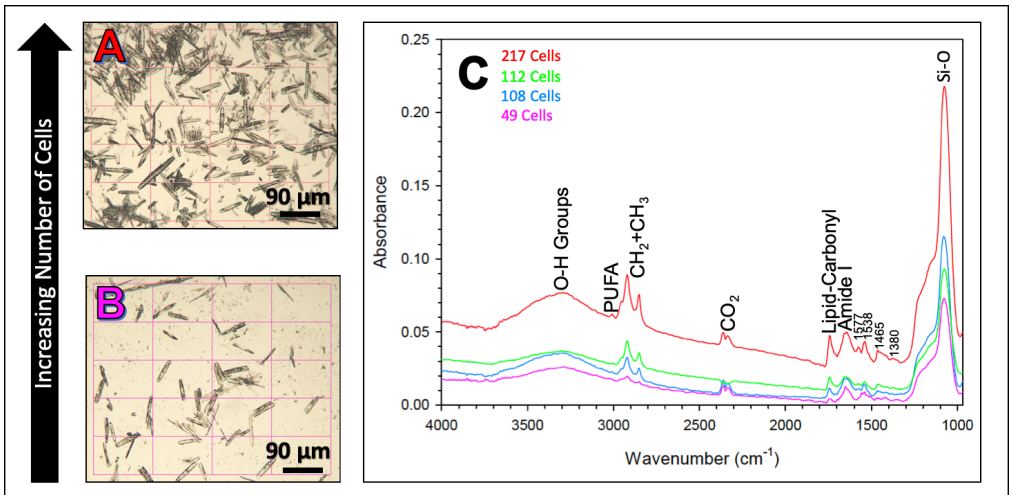


**Figure 4. 2:** An example of SE imaging highlighting cell abundance per absorbance spectrum. (A) SE field of view for 217 diatom cells, (B) SE field of view for 49 diatom cells, and (C) summed IR absorbance spectrum per number of cells within a SE field of view.

### 4.2.7 Statistical Analysis

Least-squares linear regression analysis ($y = b_0 + b_1 x$) and non-linear regression ($y = b_1 x^e$) were conducted to obtained the coefficient of determination ($R^2$) and significance (p-value) between pairs of biomass variables (i.e. number of cells, integrated FTIR band areas of Si-O, $CH_2$+$CH_3$, Amide I, and number of pixels).

## 4.4 RESULTS & DISCUSSION

### 4.3.1 0-2 cm FPA Bulk Correlation

The FPA detector bulk community 0-2 cm method was rapid, efficient, and precise in collecting bulk community biomolecular measurements, with image acquisition times ranging between 8-10 min per FOV. Least-squares linear regression analysis between the sum of

integrated Si-O (x-axis) and sum of cells (y-axis) produced a strong positive linear trend (i.e. 86% of the cell number is explained by the model: Fig. 4.3A). This strong regression is

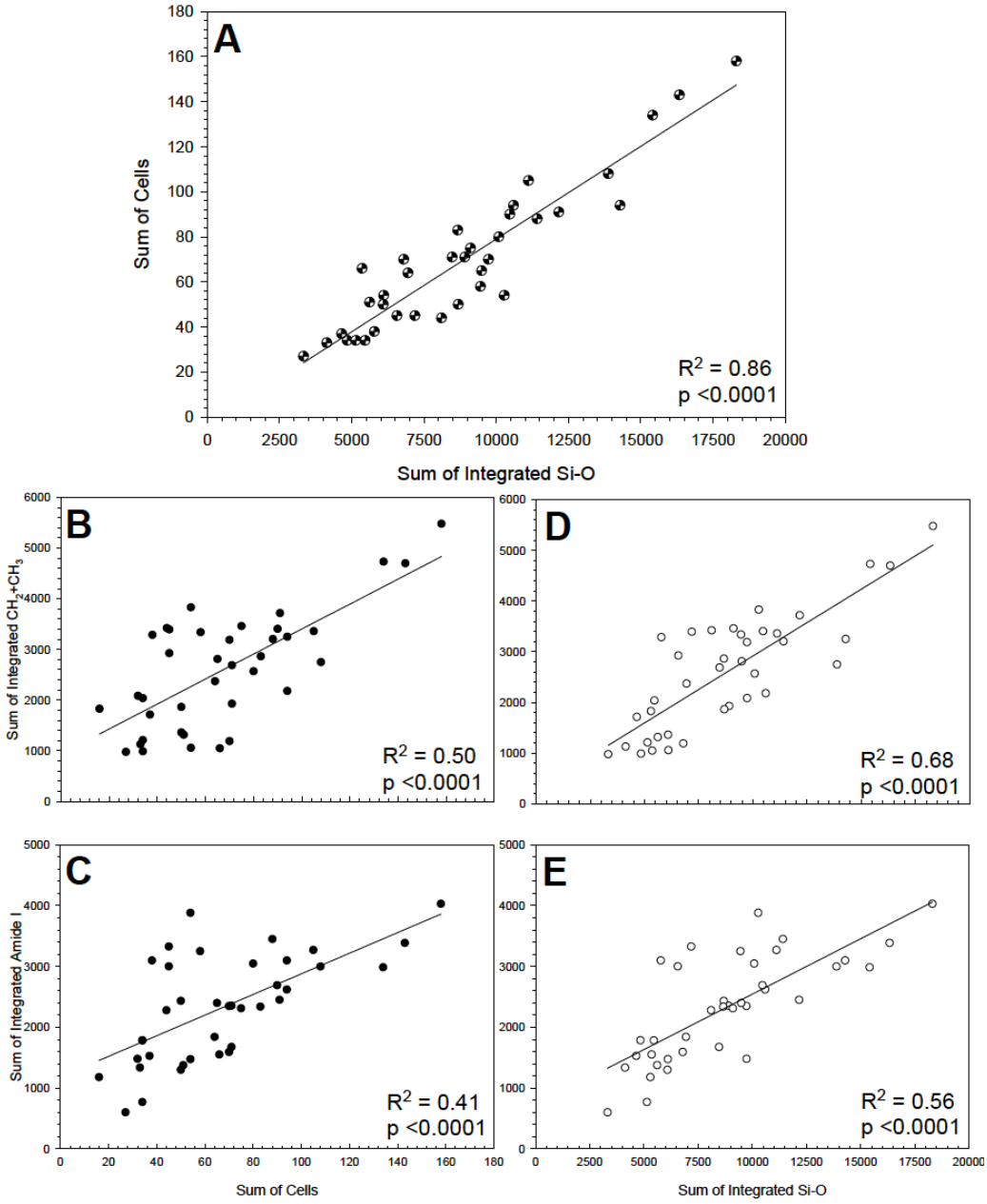


**Figure 4. 3:** FPA 0-2 cm linear correlations ($y = b_0 + b_1 x$) between (A) sum of integrated Si-O vs. sum of cells ($y = -3.21 + 0.01x$), (B) sum of cells vs. sum of integrated $CH_2$+$CH_3$ ($y = 934.10 + 24.67x$), (C) sum of cells vs. sum of integrated Amide I ($y = 1182.51 + 16.95x$), (D) sum of integrated Si-O vs. sum of integrated $CH_2$+$CH_3$ ($y = 273.47 + 0.26x$), and (E) sum of integrated Si-O vs. sum of integrated Amide I ($y = 721.24 + 0.18x$).

likely because the number of cells within a FOV directly influences the spectral Si-O absorption peak, and therefore, more cells will result in greater Si-O content (vice versa; Round et al. 1990). The sum of integrated $CH_2$+$CH_3$ (Fig. 4.3B) and Amide I (Fig. 4.3C) exhibited a significant and positive linear correlation when normalized to the sum of cells. However, the correlation between the sum of integrated Si-O and sums of integrated $CH_2$+$CH_3$ (Fig. 4.3D) and Amide I (Fig. 4.3E), displayed a stronger relationship then that with number of cells (Fig. 4.3B-C). This strong linear relationship is likely because Si-O is a measurement of integrated cell volume of biogenic silica (similar for $CH_2$+$CH_3$ and Amide I) and takes into account cell size, unlike the sum of cells variable, which carries an inherent error (i.e. cell size is not constant within a FOV).

### 4.3.2 0-10 cm FPA Single Cell Correlation

The FPA detector single cell (0-10 cm) analysis provided a more precise measurement, but was not as rapid as the FPA bulk method (0-2 cm), with image acquisition times ranging between 8-16 min per cell (cell size dependent). Single cell data analysis of the combined *Attheya* spp. and *Nitzschia frigida* biomolecular composition within a 0-10 cm sea ice layer is shown in Fig. 4.4. Non-linear regression analysis (i.e. power fit) between the sum of integrated Si-O (x-axis) and sum of pixels (i.e. number of pixels that comprise of one cell; y-axis) produced a strong positive regression (Fig. 4.4A). This is understandable as both the integrated Si-O and sum of pixels remove the diatom size factor from the equation (i.e. the number of pixels and Si-O that make-up the diatom cell is indictive of the diatom's original size). The cells that have lower pixel and Si-O values consist mainly of the centric diatom *Attheya* spp. (avg. size of 9 x 10 μm), while larger pixel and Si-O values belong to the pennate diatom *Nitzschia frigida* (avg. size of 68 x 8 μm).

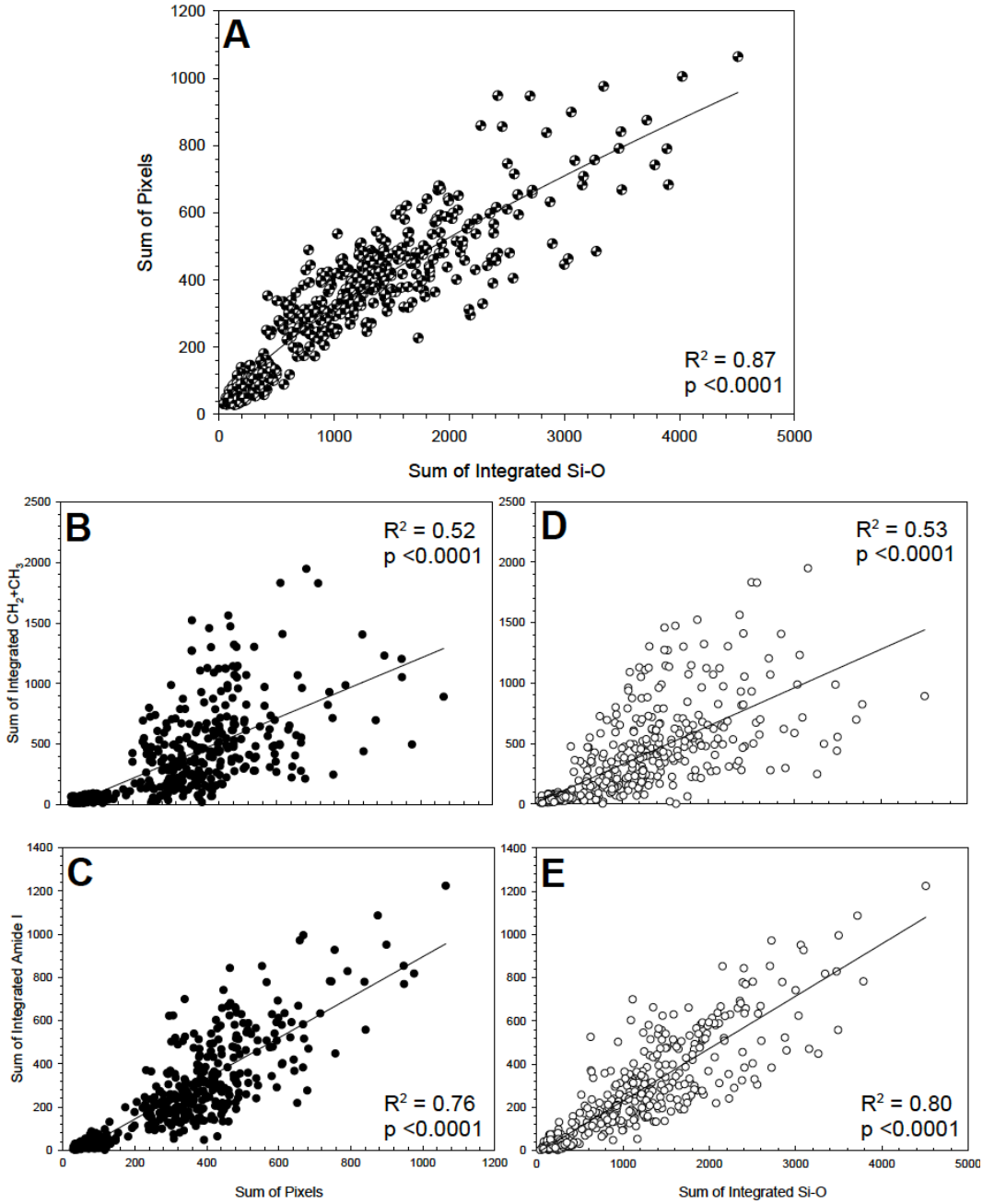


**Figure 4. 4:** FPA *Attheya* spp. and *Nitzschia frigida* 0-10 cm linear ($y = b_0 + b_1 x$) and power ($y = b_1 x^e$) correlations between (A) sum of integrated Si-O vs. sum of pixels ($y = 1.96x^{0.74}$), (B) sum of pixels vs. sum of integrated $CH_2$+$CH_3$ ($y = -30.86 + 1.24x$), (C) sum of pixels vs. sum of integrated Amide I ($y = 8.45 + 0.32x$), (D) sum of integrated Si-O vs. sum of integrated $CH_2$+$CH_3$ ($y = -42.84 + 0.94x$), and (E) sum of integrated Si-O vs. sum of integrated Amide I ($y = -13.86 + 0.25x$).

Regardless of the dependent variable (x-axis) chosen, either the sum of pixels or the sum of integrated Si-O, the sum of integrated $CH_2$+$CH_3$ (Fig. 4.4A and D) and Amide I (Fig. 4.4C and E) correlated well against both independent variables (sum of pixels and sum of Si-O). $CH_2$+$CH_3$ versus either the sum of pixels or the sum of integrated Si-O resulted in similar $R^2$ values. Similarly, Amide I versus either the sum of pixels or the sum of integrated Si-O resulted in strong $R^2$ values of 0.76 and 0.80, respectively. In essence, either parameter could serve to be used to determine $CH_2$+$CH_3$ or Amide I content on a per cell bases.

### 4.3.3 0-10 cm Single Element Bulk Correlation

The SE detection method was very rapid in comparison to both FPA methods for bulk community biomolecular measurements, with data acquisition times ranging between 2-5 min per FOV. However, the SE FOV is not well established and has only been estimated to be 530 x 440 mm. Least-squares linear regression analysis between the sum of integrated Si-O (x-axis) and sum of cells (y-axis) resulted in a positive significant linear relationship. However, the number of cells did not strongly increase with an increase in integrated spectral Si-O (*see Fig. 4.3A for cell and Si-O relationship*). This weak correlation might be due to a disconnect between the area imaged and cells counted. Additionally, the greater imaging area of the SE will include more background and debris (non-cells) signal, producing a greater error in the spectrum. In Figure 4.3B and C (0-2 FPA) the sum of cells versus the sum of the integrated $CH_2$+$CH_3$ and Amide I dataset also exhibited a weak correlation. However, the comparison between the sum of integrated Si-O (Fig. 4.5D and E) and the sum of integrated $CH_2$+$CH_3$ and Amide I content exhibited a much stronger relationship.

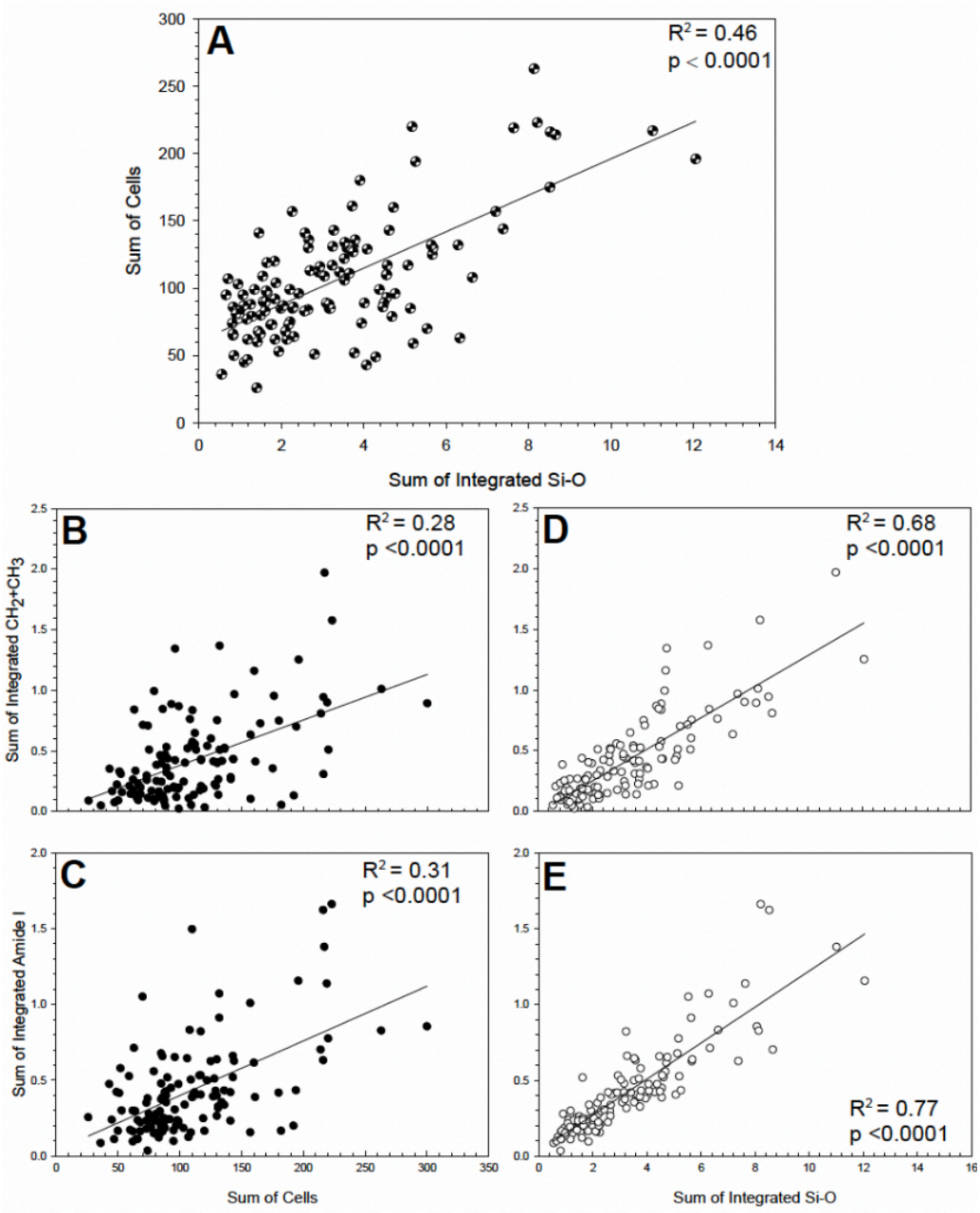


**Figure 4. 5:** SE 0-10 cm linear correlations ($y = b_0 + b_1x$) between (A) sum of integrated Si-O vs. sum of cells ($y = 60.88 + 13.53x$), (B) sum of cells vs. sum of integrated $CH_2$+$CH_3$ ($y = 0.01 + 0.004x$), (C) sum of cells vs. sum of integrated Amide I ($y = 0.04 + 0.004x$), (D) sum of integrated Si-O vs. sum of integrated $CH_2$+$CH_3$ ($y = -0.01 + 0.13x$), and (E) sum of integrated Si-O vs. sum of integrated Amide I ($y = 0.03 + 0.12x$).

Although both detectors are built into the FTIR microscope, the absorbance measurements between the two methods are dissimilar (i.e. record different absorbance values for a similar

image). Therefore, they cannot be directly compared by absorbance values. This can be improved with further direct comparison tests on the two detectors to develop a calibration or transformation method, using identical samples and imaging area (i.e. 352 x 352 μm).

## 4.4 CONCLUSION

FTIR spectrochemical imaging has previously proven to be successful in analysing the biomolecular composition of diatom cells (Giordano et al. 2001, Stehfast et al. 2005, Heraud et al. 2008, Dean et al. 2010, Sackett et al. 2013, 2016, Findley et al. 2015, Pogorzelec et al. 2017). Here, we presented three different methods that would be suitable for of measuring the biomolecular composition of the diatom community in a rapid, efficient, and precise manner. Each method has its own particular set of pros and cons. For instance, both FPA methods give similar image acquisition times of 8-10 min and are comparable to the results observed in *Chapter 3*. The FPA bulk community method (5.5 x 5.5 μm pixel resolution or normal mag.) results in a larger imaging area and the ability to capture multiple cells, while the FPA method for individual cell analysis (1.1 x 1.1 μm pixel resolution or high mag.) cannot. Though the FPA individual cell method likely yields more accurate results, due to the exclusion of the background in summed biomolecular composition, the increased time would make this method inefficient for bulk analysis. The SE bulk community method provides a much larger FOV and faster image acquisition time by ~ 2-5 min per sample but did not reproduce the same quality of results as observed in *Chapter 3*. Therefore, we believe the FPA bulk community (normal mag.) method is best for acquiring bulk community biomolecular composition in a precise and efficient manner. This is because the FPA bulk community method has a smaller FOV and, thus, removes most of the background error in the summed measurements (observed in SE method). It also closely

follows the measurements that were presented in *Chapter 3* for single cell analysis. However, more testing is required to truly determine the best bulk analysis method, via FTIR spectrochemical imaging.

# 4.5 REFERENCES


Arrigo, K.R., (2014) Sea ice ecosystems. Annu. Rev. Mar. Sci., 6:439-67. doi: 10.1146/annurev-marine-010213-135103

Comiso, J.C., Parkinson, C.L., Gersten, R. and Stock, L., (2008) Accelerated decline in the Arctic sea ice cover. Geophys. Res. Lett., 35: L01703. doi: 10.1029/2007GL031972

Dalman, L.A., Else, B.E., Barber, D., Carmack, E., Williams, W.J., Campbell, K., Duke, P.J., Mundy, C.J., (2019) Enhanced bottom-ice algal biomass along a tidal strait in the Kitikmeot Sea of the Canadian Arctic. Elementa (Accepted 2019)

Dean AP, Sigee DC, Estrada B, Pittman JK (2010) Using FTIR spectroscopy for rapid determination of lipid accumulation in response to nitrogen limitation in freshwater microalgae. Bioresource Technol 101: 4499−4507

Findlay CR, Wiens R, Rak M, Sedlmair J, Hirschmugl CJ and others (2015) Rapid biodiagnostic ex-vivo imaging at 1 μm pixel resolution with thermal source FTIR FPA. Analyst 140:2493 – 2503

Garrison, D.L. and Buck, K.R., (1986) Organism losses during ice melting: a serious bias in sea ice communities studies. Polar Biol 6:237-239

Giordano, M., Kansiz, M., Heraud, P., Beardall, J., Wood, B., and McNaught, D., (2001) Fourier transform infrared spectroscopy as a novel tool to investigate changes in intracellular macromolecular pools in the marine microalga Chaetoceros Muellerii (Bacillariophyceae). J. Phycol. 37:271-279

Gosselin, M., Legendre, L., Therriault, J.C. and Demers, S., (1990) Light and nutrient limitation of sea-ice microalgae (Hundson Bay, Canadian Arctic). J. PhycoL, 26:220-232

Griffiths P, de Haseth J (2007) Fourier Transform Infrared Spectrometry, 2nd edn. Wiley Inter-Science, New Jersey

Heraud P, Stojkovic S, Beardall J, McNaughton D, Wood BR (2008) Intercolonial variability in macromolecular composition in P-starved and P-replete Scenedesmus populations revealed by infrared microspectroscopy. J Phycol 44: 1335−1339

Leu E, Wiktor J, Søreide JE, Berge J, Falk-Petersen S (2010) Increased irradiance reduces food quality of sea ice algae. MAR ECOL-PROG SER 411:49-60

Leu, E., Mundy, C.J., Assmy, P., Campbell, K., Gabrielsen, T.M., Gosselin, M., Juul-Pedersen, T. and Gradinger, R., (2015) Arctic spring awakening-steering principles behind the phenology of vernal ice algae blooms. Progress in Oceanography, 139:151-170

Markus, T., Strieve, J.C., and Miller, J., (2009) Recent changes in Arctic sea ice melt onset, freezeup, and melt season length. Journal of Geophysical research, 114:C12024

Michel, C., Ingram, R.G., Harris, L.R. (2006) Variability in oceanographic and ecologicl processes in the Canadian Arctic Archipelago. Progress in Oceanography, 71:379-401

Mock, T., and Gradinger, R., (2000) Changes in photosynthesis carbon allocation in algal assemblages of Arctic sea ice with decreasing nutrient concentration and irradiance. Mar Ecol-Prog Ser, 202:1-11

Mock, T., and Kroon B., (2002a) Photosynthetic energy conversion under extreme conditions-I: important role of lipids as structural modulators and energy sink under N-limited growth in Antarctic sea ice diatoms. Phytochemistry, 61:41-51

Mock, T., and Kroon, B., (2002b) Photosynthetic energy conversion under extreme conditions-II: the significant of lipids under light limited growth in Antarctic sea ice diatoms. Phytochemistry, 61:53-60

Mock, T., Thomas, D.N., (2005) Recent advances in sea-ice microbiology. Environmental Microbiology, 7(5):605-619

Pogorzelec, N.M., Mundy, C.J., Findlay, C.R., Campbell, K., Diaz, A., Ehn, J.K., Rysgaard, S. and Gough, K.M., (2017) FTIR imaging analysis of cell content in sea-ice diatom taxa during a spring bloom in the lower Northwest Passage of the Canadian Arctic**.** MEPS, 69:77-88

Poulin, M., Daubjerg, N., Gradinger, R., Ilyash, L., Ratkova, T., and von Quillfedt, C., (2011) The pan-Arctic biodiversity of marine pelagic and sea-ice unicellular eukaryotes: a first-attempt assessment. Mar. Biodiv., 41:13-28

Rintala, J.M., Piiparinen, J., Blomster, J., Majaneva, M., Müller, S., Uusikivi, J. and Autio, R., (2014) Fast direct melting of brackish sea-ice samples results in biologically more accurate results than slow buffered melting. Polar Bio, DOI 10.1007/s00300-014-1563-1

Round, F., Crawford, R., and Mann, D., (1990) Diatoms: biology and morphology of the genera. Cambridge University Press.

Sackett O, Petrou K, Reedy B, De Grazia A and others (2013) Phenotypic plasticity of Southern Ocean diatoms: key to success in the sea ice habitat? PLOS ONE 8: e81/85

Sackett O, Petrou K, Reedy B, Hill R and others (2016) Snapshot prediction of carbon productivity, carbon and protein content in Southern Ocean diatom using FTIR spectroscopy. ISME J 10: 416−426

Sattar, A. and Alexander, J.C., (1976) Effect of wavelength on light induced quality of deterioration of edible oils and fats. Can. Inst. Food Sci. Technol. J. 9:180-113

Søreide, J.E., Leu, E.V.A., BERGE, J., Graeve, M. and Falk-Petersen, S.T.I.G., (2010) Timing of blooms, algal food quality and Calanus glacialis reproduction and growth in a changing Arctic. Global Change Biology 16:3154-3163

Stitt DM, Kastyak-Ibrahim MZ, Liao CR, Morrison J, Albensi BC, Gough KM (2012) Tissue acquisition and storage associated oxidation considerations for FTIR microspectroscopic imaging of polyunsaturated fatty acids. Vibrational Spectroscopy 60:16-22

Stroeve, J.C., Serreze, M.C., Holland, M.M., Kay, J.E., Malanik, J., and Barrett, A.P., (2012) The Arctic's rapidly shrinking sea ice cover: a research synthesis. Climate Change 110:1005-1027, doi 10.1007/s10584-011-0101-1

# CHAPTER 5: CONCLUSION & RECOMMENDATIONS

## 5.1 CHAPTER SUMMARY

Chapter 1 briefly introduces the thesis topic and outlines the general goals, thesis objectives, and hypotheses. Chapter 2 illustrates a detailed, but brief literature review that includes referenced material describing ice algal habitat and characteristics (i.e. location within sea ice, seeding/colonization mechanisms and dominant ice algal taxa). The review also briefly discusses the role of light availability and nutrient cycling mechanisms as well as how ice algae are influenced by these environmental factors. Lastly, the chapter ends with a description of Fourier Transform Infrared Spectrochemical imaging and the various techniques that can be used to monitor the biomolecular composition of ice alga cells.

Chapter 3 is the first of two data chapters, consisting of a manuscript in final preparation for submission to the international journal, *Elementa: Science of the Anthropocene*. It examines changes in the biomolecular composition of individual diatom cells exposed to two expected nutrient supply gradients in their natural environment: (1) a spatial gradient across a tidal strait and (2) a vertical gradient up into the bottom ice matrix. Diatom samples were collected from the bottom-ice 0-10 cm section (0-2, 2-5, and 5-10 cm) along a transect across a tidal strait between the Finlayson Islands (Dease Strait, near Cambridge Bay, NU, CA). We hypothesized that an increase in ocean-ice nutrient supply would occur towards the centre of the strait where sub-ice currents and turbulence were greatest (Dalman et al. 2019). Two diatom taxa, *Nitzschia frigida* and *Attheya* spp., were selected for Fourier Transform Infrared (FTIR) spectrochemical analysis for lipid and protein content. The existence of spatial and vertical nutrient gradients across the Finlayson Island tidal strait was strongly supported by trends and differences observed in cellular

biomass composition, estimated via the FTIR technique. In contrast, bulk measurements (e.g., nutrient concentrations, particulate organic carbon (POC) and POC:Chl *a*) were difficult to interpret with respect to a spatial trend, except for chlorophyll *a* (Chl *a*) concentration. However, all bulk measurements detected a vertical nutrient gradient into the bottom-ice matrix. The larger pennate diatom, *N. frigida*, was more sensitive to the spatial gradient where lipid (protein) increased (decreased) and the lipid:protein ratio increased towards the outside of the tidal strait (i.e. site 4). The non-motile diatom, *Attheya* spp., was observed to be more sensitive to the vertical gradient (i.e. exhibited greater change in the cellular lipid:protein ratio). It was surmised that *Attheya* spp. cells were likely trapped above the 0-2 cm ice section with very limited nutrient supply. The FTIR technique proved to be a powerful technique to observe individual diatom sensitivity to nutrient supply, seen as changes in biomolecular composition along spatial and vertical nutrient gradients.

Chapter 4 is the second of the data chapters. It evaluates and compares three different FTIR methods that are capable of examining the bulk diatom community in a rapid and efficient manner. The diatoms cell wall consists of a glass-like matrix composed of biogenic silica, called a frustule. FTIR spectrochemical imaging has continued to prove to be a successful technique for measurement of the biomolecular composition of diatom cells. However, the speed at which FTIR diatom image acquisition is accomplished has the potential to be greatly improved. Diatom section samples were collected between the Finlayson Islands within the Dease Strait, near Cambridge Bay, NU, CA. Out of the three techniques examined, the FPA 0-2 cm bulk community (normal magnification) method was determined to be the most optimal method in measuring bulk community biomolecular composition in a short period of time, as well as being closely relatable to the single cell high magnification FTIR analysis data observed in Chapter 3.

Chapter 5 concludes this thesis by summarizing the key conclusions and providing future recommendations for the application of FTIR spectroscopy in support of ice algae, and more generally, diatom autecological research.

## 5.2 FUTURE RECOMMENDATIONS & CONCLUSIONS

With climate change rapidly affecting the Arctic icescape (i.e. decreasing sea ice extent and thickness, earlier melt, and later freeze-up), more research is urgently needed to better understand how these changes will impact the important ice algal community and their annual spring bloom. My thesis research identified trends in diatom taxa sensitivities to natural nutrient gradients. From this research, there are still open questions and potential future avenues of research that will help improve our understanding of ice algal dynamics and the application of FTIR imaging to diatom autecological research. Below are future research recommendations that I suggest will push forward the research presented in this thesis.

i. In order to fully identify key patterns and trends between primary producers and their natural environment, two experimental studies are recommended: (1) new FTIR time series data collection and (2) a controlled light-nutrient exposure experiment.

Experiment 1: The tidal strait experiment in Chapter 3 should be re-visited for different regions across the Arctic, with a few minor modifications:

a. Similar to Chapter 3, ice cores can be collected along a tidal strait region and segmented into 0-2, 2-5 and 5-10 cm ice sections. However, the number of sites sampled should be increased in order to capture tighter transitional trends between sites.

b. Under-ice nutrients and intra-cellular nutrients should be collected in addition to in-ice nutrients. These additional nutrient measurements will serve as a baseline to help set nutrient concentrations for the controlled experiment (part 2).
c. The study should measure under-ice currents to establish a better understanding of its relationship to nutrient fluxes and incorporation into the bottom ice.

Experiment 2: The second part of this recommendation is an experiment to examine the epiphytic-host relationship between *Attheya* spp. and pennate diatoms. The observed increase in nutrient stress among *Attheya* spp. cells (non-motile) further into the sea-ice matrix was surmised to be influenced by not only the loss of the host diatom, but also cell entrapment with no new nutrient supply. To test these relationships, I suggest to undertake a controlled laboratory culture experiment to examine the direct impact of varying light and nutrient stress on *Attheya spp.*, *N. frigida*, and the two taxa together. Figure 5.1 illustrates the basic outline for the controlled culture experiment (or multifactorial experiment):

a. Light, nutrients, temperature and salinity would be monitored and controlled to match as best as possible the parameters observed within the bottom-ice habitat.
b. Diatom groups of *Attheya* spp., *N. frigida*, and both taxa together are to be exposed to the different treatments (Fig. 5.1).
c. Cultured diatoms from each group and treatment would be sampled regularly over the course of a 1- to 2-week period and analyzed by FTIR spectrochemical imaging. Changes observed within the biomolecular composition of the diatom groups should help confirm and expand upon the diatom-diatom relationship and cell entrapment theory that was initially suggested in Chapter 3.

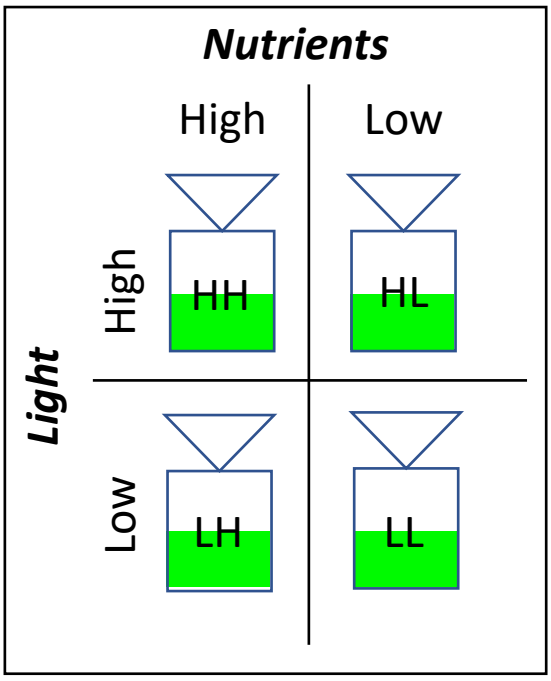


**Figure 5. 1:** Cultured based experiment for examining *Attheya* spp. and *N. frigida* epiphytic-host relationship under different light and nutrient treatments.

ii. The successful rapid FTIR technique presented in Chapter 4 will serve as a precursor in developing a method that will allow seamless comparison between two separate FTIR detectors (SE and FPA). This can be easily accomplished by imaging a series of identical algal samples, switching between detectors (i.e. Single Element (SE) and Focal Plane Array (FPA)) and adjusting the microscopes' field of view to be more comparable.

iii. Chapter 4 also gave rise to the consideration of developing a prediction model/ calibration curve for determining absolute concentrations of single celled diatoms' biomolecular composition (i.e. lipid, protein, and bio-genic silica), instead of the relative values presented in this Thesis. This is in fact possible for bulk community samples, as reported in Wagner et al. 2010, and Laurens and Wolfrum 2011. The authors were able to determine absolute concentrations of biomolecular content, via FTIR, that were comparable to other chemometric analyses (e.g. HPLC). This would provide for a more

rapid and accurate comparison with other traditional analytical techniques and would offer an opportunity to construct a method for rapidly determining the absolute concentration of biomolecular content within individual algal cells.

iv. Lastly, a future project should focus on further exploring the relationship between POC:PON (particulate organic carbon and particulate organic nitrogen) and the lipid:protein ratio ($CH_2$+$CH_3$:Amide I; 0-10 cm), in order to construct a universal calibration curve. Wagner and Jebsen (2019) observed a strong relationship between measured carbon:nitrogen ratios and FTIR related lipid:protein peak ratios, which was also observed below in Figure 5.1 ($R = 0.87$ and $R^2 = 0.75$) using the SE bulk community measurements (*method in Chapter 4*) and POC:PON measurements (Elemental Analyzer (*Elementar Vario Micro Cube*); Cutter et al. 2014).

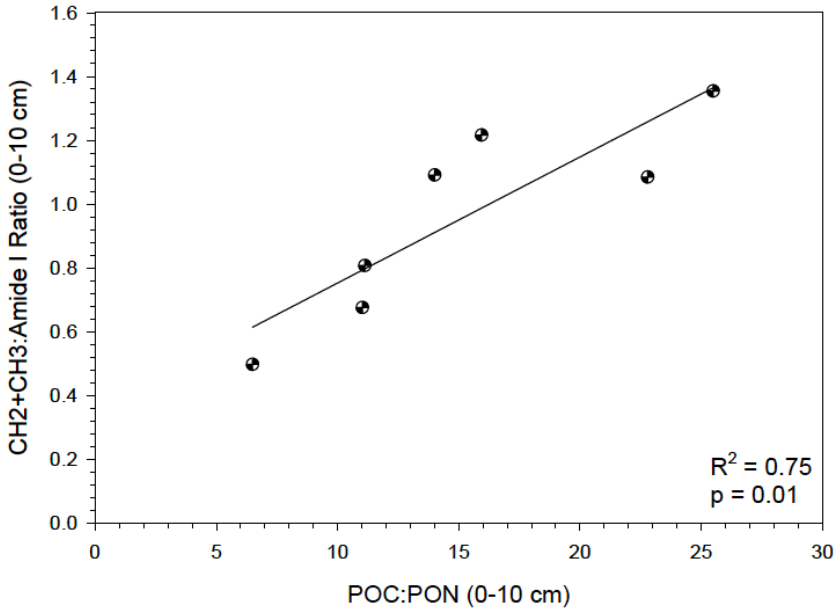


**Figure 5. 2:** Linear correlation ($y = b_0 + b_1 x$) between POC:PON ratio and SE bulk community $CH_2$+$CH_3$:Amide I ratio 0-10 cm ($y = 0.36 + 0.04x$).

These proposed future research recommendations will provide further insight on the ice algal community, pushing forward the studies presented in this M.Sc. thesis. Ice algae are a critical component within the Arctic marine ecosystem, yet a lack of understanding has impeded our ability to predict the ecosystem's response to ongoing climate change. This M.Sc. thesis has provided new understanding and insight into the ice algal community and how individual diatom cells respond, via biomolecular composition, to spatial and vertical nutrient gradients within a tidal strait area. This M.Sc. thesis has also presented new imaging techniques that can rapidly measure the biomolecular composition of the ice algal community. This has expanded upon the possibility of creating new experiments to increase measurement efficiency, accuracy and precision. The new information presented here has significantly increased our understanding of the ice algal community and will help us better to predict future responses of this community to a constantly changing environment.

# 5.3 REFERENCES


Cutter, C., Andersson, P., Codispoti, L., Croot, P., Francois, R., Lohan, M.C., Obata, H. and Rutgers van der Loeff, M., (2014) Sampling and sample-handling protocols for GEOTRACES cruises, v. 2.0., GEOTRACES, pp 123-125

Dalman, L.A., Else, B.E., Barber, D., Carmack, E., Williams, W.J., Campbell, K., Duke, P.J., Mundy, C.J., (2019) Enhanced bottom-ice algal biomass along a tidal strait in the Kitikmeot Sea of the Canadian Arctic. Elementa (Accepted 2019)

Pogorzelec, N.M., Mundy, C.J., Findlay, C.R., Campbell, K., Diaz, A., Ehn, J.K., Rysgaard, S. and Gough, K.M., (2017) FTIR imaging analysis of cell content in sea-ice diatom taxa during a spring bloom in the lower Northwest Passage of the Canadian Arctic**.** MEPS, 69:77-88

Laurens, L.M.L., and Wolfrum, E.J., (2011) Feasibility of spectroscopic characterization of algal lipid: chemometric correlation of NIR and FTIR spectra with exogenous lipids in algal biomass. Bioenerg. Res. 4:22-35

Wagner, H., and Jebsen, C., (2019) Monitoring cellular C:N ratio in phytoplankton by means of FTIR-spectroscopy. J. Phycol. DOI: 10.111/jpy.12858

Wagner, H., Liu, Zhixin., Langner, U., Stehfest, K., and Wilhelm, C. (2010) The use of FTIR spectroscopy to assess quantitative changes in the biochemical composition of microalgae. J. Biophoton. 3(8-9):557-566